Cellulose Reinforced PCL Biomimetic Nanocomposites for Bone Tissue Engineering

Laraib Abbas

00000321280

A thesis submitted in partial fulfillment of the degree of

Master of Philosophy

in

Chemistry

Supervised by: Dr. Mudassir Iqbal

Department of Chemistry

School of Natural Sciences

National University of Sciences and Technology

H-12, Islamabad, Pakistan

2021.

FORM TH-4

National University of Sciences & Technology

MS THESIS WORK

We hereby recommend that the dissertation prepared under our supervision by: Laraib Abbas, Regn No. 00000321280 Titled: Cellulose reinforced Poly caprolactone bio mimetic nanocomposites for bone tissue engineering applications be Accepted in partial fulfillment of the requirements for the award of **MS** degree.

Examination Committee Members

1. Name: DR. AZHAR MAHMOOD Signature: _____

2. Name: DR. FAHEEM AMIN Signature: _____

External Examiner: DR. SYEDA AALIYA SHEHZADI Signature: _____

Supervisor's Name DR. MUDASSIR IQBAL Signature: _____

Co-Supervisor's Name DR. M. ADIL MANSOOR Signature: _____

_____ 14/2/22

Head of Department Date

COUNTERSINGED

Date: 14.2.2022

Dean/Principal

Dedicated to my Beloved Parents

for their Endless Love, Support and Encouragement!!

Table of Contents

List of Abbreviations

BTE	Bone Tissue Engineering
PCL	Poly-Caprolactone
MCC	Micro Crystalline Cellulose
WH	Whitlockite
HA	Hydroxyapatite
TCP	Tri Calcium Phosphate
BCP	Bi Calcium Phosphate
PBS	Phosphate Buffer Saline
ECM	Extra cellular matrix
DMEM	Dulbecco’s modified eagle medium
FBS	Fetal Bovine Serum
MTT	Methyl Tetrazolium
hMTSC	Human Mesenchymal stem cells
UTS	Ultimate Tensile Strength
SEM	Scanning Electron Microscopy
mL	Mililiter
µL	Microliter
µm	Micro meter

List of Figures

List of Tables

Acknowledgements

First of all, I would like to bow before **Almighty ALLAH**, the most merciful, the most Beneficial Who bestowed me with such a lucid intelligence as I could endeavor my services towards this manuscript. Then I pay all my respect to the greatest man of the universe, the **Holy Prophet MUHAMMAD (S.A.W)** whose life and wordings are ultimate source of guidance and way of "Nijat" for mankind.

It seems impossible to pay thanks to my father **Muhammad Abbas** and my mother **Bushra Abbas** for their continuous support and guidance throughout my life and encouraging me to pursue higher education. I immensely appreciate the love, care and constant nagging from my brothers **Babar Abbas** and **Behram Abbas**.

It is my privilege and honor to express my gratitude to my research supervisor **Dr. Mudassir iqbal,** National University of Science and Technology, for his constructive supervision during the accomplishment of this thesis. I admire his patience, tenderness, devotion and intellectual supervision to spread knowledge and promote innovation.

I am thankful to my co-supervisor **Dr. Muhammad Adil** for his kind support and his valuable suggestions for writing this thesis. I am grateful to all my GEC members **Dr. Azhar Mahmood,** and **Dr. Faheem.** I thank all my teachers for their guidance and staff members (technical and administrative) at SNS for their help at various stages during my MS journey.

I extend my gratitude to **Dr. Farzana Nazir** whose guidance and kindness was much help during my whole research work. I have been lucky one for having my friends by my side during this whole process.

Abstract

This research project is based on the concept of elucidating development procedure of fabricating novel biomimetic nanocomposites for the application of bone tissue engineering and whose mechanical, morphological, compositional, biocompatible properties are compared with that of natural bone. These biomimetic nanocomposites are composed of biopolymer matrix in which nHA and nWH nanoparticles are embedded. Biopolymers such as PCL and MCC constitute the hybrid base matrix and effect of different weight ratios of nHA and nWH on the chemical, physical and mechanical properties of nanocomposites was investigated.

Nanoparticles nHA and nWH were chemically synthesized by wet chemical precipitation and tri solvent system respectively. Nanoparticles were aged and calcined to regulate the growth of their size and morphology. These synthesis methods were based on aqueous systems and offered control over the size and morphology of the nanoparticles. Blends of PCL and MCC are prepared by taking 5-15% of MCC with subsequent PCL matrix using solvent casting method. Tensile strength evaluation suggested PCL/MCC-5 blend composition for further nanoparticle addition. Nanoparticles were dispersed into biopolymer blends by adopting solvent casting technique and nanocomposites with different weight loadings of nHA and nWH were successfully prepared.

Effect of altering weight loading on the nanocomposites were evaluated and characterized through Compression testing, Scanning Electron Microscopy, Fourier Transform Infrared Spectroscopy, X-ray diffraction, Biocompatibility testing using cell lines and swelling assay. SEM was carried out to study the morphological characteristics while compression

testing was carried out to optimize and evaluate mechanical strength. Cell culture was performed on vero cell line to investigate biocompatibility of these nanocomposites.

This study revealed that mechanical properties of the polymer blends can be enhanced on the addition of nanoparticles and optimized to make it comparable to that of natural bone. Cell viability data shows that biocompatibility on the whole is around 85% and with inclusion of nanoparticles it reaches upto 95%. These results demonstrate that hybrid polymer nanocomposites possess desirable biocompatibility and tensile strength that make them a promising bone implants.

Chapter 1

1 Introduction:

1.1 Nanotechnology:

Development and designing of well oriented and regimented nanostructure material by either bottom up or top down approach which are greatly receptive to outer stimuli, is referred as nanotechnology. Owing to scientist's growing interest to scrutinize things at nano scale, a new hybrid science, combining both nanotechnology and biotechnology, has emerged which involves incorporation of modified and functionalized nanostructures and is manifested as nano-biotechnology. In biomedicine, it has huge applications that spans over vast area such as diagnosis, drug design, therapy and design of load bearing implants. Nanomaterial is integrated efficiently into biomedical designs as most of the biological structures like bacteria, viruses and biomolecules are in nanometer range. Nano-biotechnology has been utilized to fabricate microchips, biosensors, and tissue substitutes for skin, bone and muscles. It has gained due attraction in the biomedical ground due to enhanced surface roughness and surface area which upon external stimuli show increased osteoconductivity and osteogenicity resulting in effective implant-tissue interlocking [1]. In addition to this, improved strength and hardness of these nanomaterials also make them a potential candidate for making wear resistance scaffolds. Conjugation of bio specific molecules through nanoparticles is done by physical, chemical, and biological methods such as antigen-antibody interface, ligand- receptor interaction and DNA hybridization. As the 90% of the total mass on the surface of nanosized systems represents their concentration

and hence their reactivity. Thus, depending upon the specific end function, their surface can be modified in different ways to obtain distinct functionalities, specific biological characteristics and enhanced solubility. Applications of nanomaterial can be fine-tuned by surface physics, surface chemistry and through surface thermodynamics [2]. Research in nano biotechnology is going to revolutionize disease treatment and diagnosis methodologies in foreseeable future. Currently, it has been applied to uncover its potential usage in tissue implants and modification of nanomaterial topography. In the present research, polymeric blends of nano ceramic composites have been fabricated for bone implants and their properties have been studied. Fig.1.1 represents schematic diagram of different application areas of nano biotechnology.

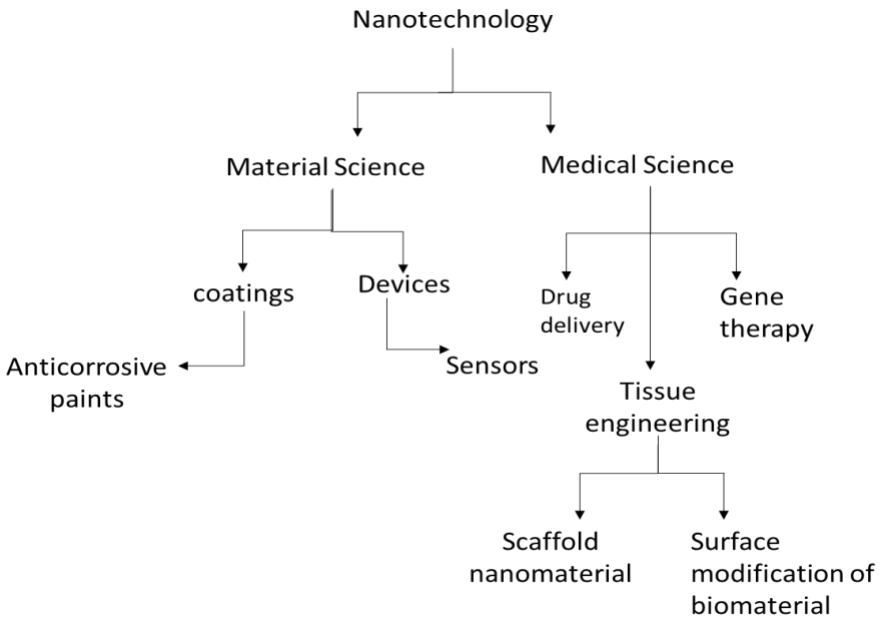

Figure 1.1 Scheme of applications of nano biotechnology in different areas

1.2 Nanocomposites:

Nanocomposites in the broadest sense refer to the multiphase solid material, in which at least one dimension of the filler is in nanometer range. Filler particles are homogeneously dispersed in the polymer matrix. These filler particles act as reinforcing agent and synergistically improve individual properties of composite components, while retaining their uniqueness. Non homogenous dispersion of nano filler can lead to agglomeration and lowered wetting of the filler particles. Depending on the type of interaction between polymer and filler, there are types of composites[3].

I. Phase separated composites:

In phase separated nanocomposites, no separation of filler particles occur and filler is present in its original form like tactoids or aggregates of tactoids. Polymer matrix and filler are immiscible and this structure exists in micrometer range.

II. Intercalated nanocomposites:

Here, polymer chains are intercalated between nano fillers and make alternating matrix-filler nanostructure while original configuration of the polymer is retained. Overall, stacking arrangement of polymer matrix is not disturbed.

III. Exfoliated nanocomposites:

In this structure, matrix chains are thoroughly exfoliated and filler particles are completely dispersed in the polymer chains giving a homogenous solution. It occurs in nanometer range.

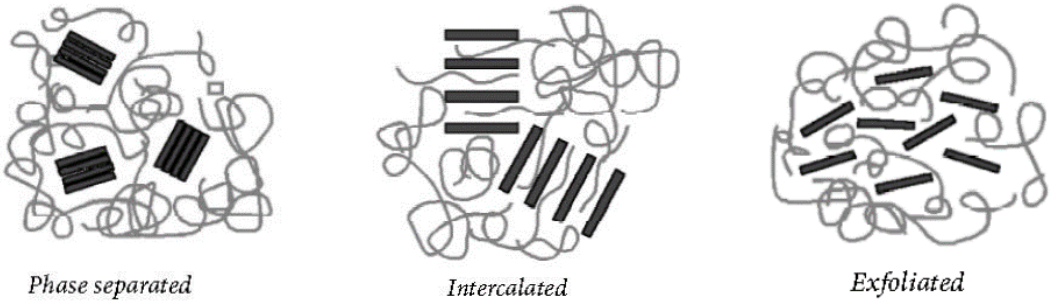

Figure 1.2 Different structures of nanocomposites

1.2.1 Selection of nanocomposite scaffold:

The criteria for the selection of scaffold material relies upon many parameters such as nature and morphology of tissue where scaffold is to be planted, biodegradability and bioresorbable etc. Following are the pre-requisites of choosing an ideal scaffold material [4].

I. Biocompatible: It creates an environment for the cell to attach, proliferate, segregate and differentiate. It eliminates after degrading into less toxic material.

II. Biodegradable: Rate of degradation is antagonistic to rate of tissue formation so, scaffold material should have a controlled degradation rate.

III. Surface topography: Suitable surface topography is pre-requisite to provide cell adhesion and cell attachment atmosphere.

IV. Porous structure: Scaffolds should have porous volume to facilitate cell's migration, nutrient's and waste transfer and other controlling factors like growth hormones. Interconnected porous network is indispensable for tissue growth.

V. Immunogenicity: It should have ability to provoke immune system to produce necessary antibodies.

VI. Mechanical strength: Mechanical strength of the scaffold material should be comparable to the tissues present at the site of implantation.

VII. Swelling: Regulated swelling of the scaffold material is necessary for the maximum nutrient and growth factor absorption.

1.3 Scaffold Fabrication methods:

Composite materials syndicate the desirable properties of two or more materials to create a scaffold which can better cater to the necessities of host cells. The basic purpose of scaffold generation is to promote and assist tissue regeneration and for that they had to meet different requirements like interconnectivity, microstructure and porosity. There are many both conventional and modern methods of 2D and 3D scaffold production which are briefly discussed as follows:

1.3.1 Solvent casting:

It is one of the simplest methods for the scaffold generation. It saves time, cost and offers controlled porosity. Polymer and filler are homogeneously spread in the suitable solvent and poured into the pre-decided mold. Only drawback of using this method is presence of solvent acting as impurity if it is not evaporated properly.

1.3.2 Electrospinning:

Discovered in the last decade, electrospinning involves creating ultrathin and greatly interconnected fibers under electric field. It suffers from disadvantage of reduced scaffold thickness and low productivity.

1.3.3 Gas foaming:

Gas foaming is the method of generating synthetic composites in which no solvent is used. It results in solvent free and porous composites but with limited interconnectivity and poor pore structure.

1.3.4 Freeze drying:

It is modern technique which in contrast to conventional drying, gets rid of solvent by reducing temperature. Resulting scaffolds are solvent free, porous and vastly interconnected. It is expensive and mechanical strength is compromised due to small pore size.

1.4 Biopolymers:

Biopolymers are the naturally occurring polymeric bio-materials which are synthesized from plants, animals, fungi and bacteria or those materials which are manufactured using bio-molecules like natural fats, sugar, and protein. They are organic in nature and are made up of monomers which are linked through covalent bonds. Depending upon the nature the source, biopolymers can be classified into two categories:

Natural biopolymers: these occur in living organisms and are animal, plant and microbe derived polymers. Depending on the type of monomer they are categorized as polysaccharides, polypeptides, and polynucleotides. Polysaccharides have carbohydrate moieties which are joined by glycosidic linkages. In proteins amino acid act as monomeric unit which are linked via peptide bonds. Polynucleotides like DNA and RNA comprise of nucleotide monomers and are heterogeneous in nature. [5]

Synthetic biopolymers: these are manmade biopolymers through abiotic chemical pathways. They include polyethylene, polyesters and polyamides. These have further two

types: degradable like PGA, PLA, PDS, PCL, PHB, PPF and non-degradable such as PE, PP, PC, PVC, PMMA,PTFE.[6]

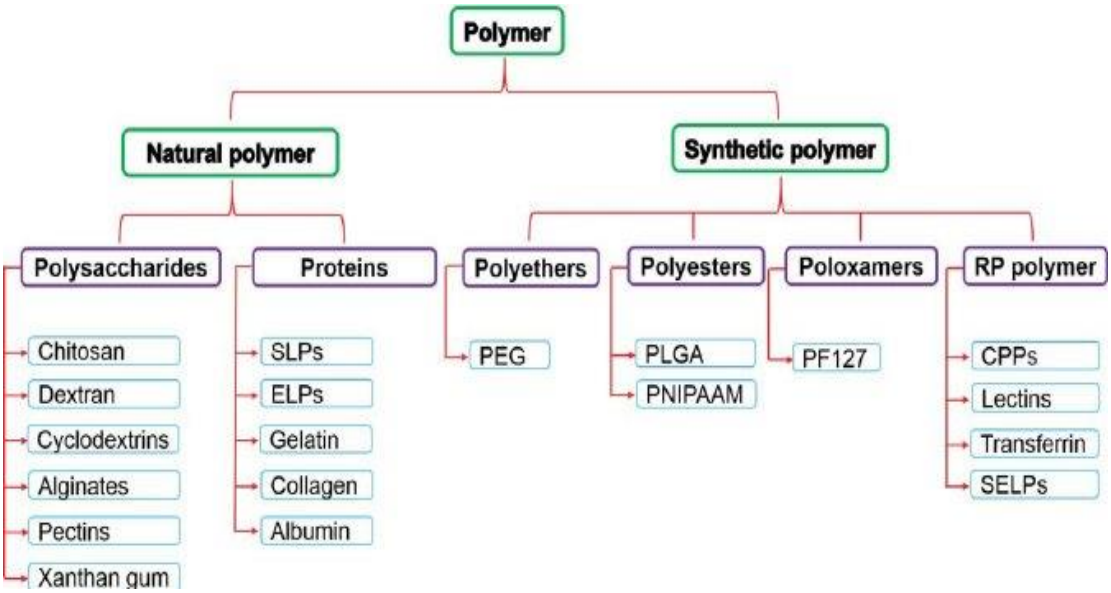

Figure 1.3 Classification of polymers

From the past few decades scientists have found extensive applications of the biopolymers in the multiple fields of science and technology. Currently, they are being used in the arenas of food industry[7], agriculture[8], nanomaterial fabrication[9, 10], water purification[11], packaging[12, 13] and biomedical purposes[14]. Their wide range usage can be attributed to their unique properties such as eco-efficiency, renewability, and sustainability. In addition to this, they are ecofriendly, reduce dependency on fossils, impede carbon dioxide emission, and waste generation.

In biomedical, biopolymers have been greatly exploited and have found applications in the pharmaceuticals, tissue engineering, drug delivery and diagnosis. 90% of the existing literature on biopolymers is primarily driven by biomedical and healthcare sciences thus,

depicting an upsurge in its demand. Biopolymers have intrinsic characteristics like biocompatibility, biodegradability and sometimes antimicrobial which paves their way in tissue engineering domain. Their physical and chemical structure recapitulate innate tissue mechanics by mimicking topography of native extra cellular matrix (ECM). Unlike synthetic polymers, natural biopolymers do not cause cytotoxicity, inflammation and autoimmune disorder when brought in contact with the living organisms[15]. Depending on the type of application, different physical and chemical methods have been applied to tailor and fine tune their biological properties such as mechanical strength, degradation etc.

Among bio-based materials, hydrogels has huge potential as a tissue engineering material as they provide an aqueous environment and also mimics ECM. ECM consists of three dimensional network of glycoproteins, collagen and enzymes that collectively support to the surrounding cells and tissues. However, hydrogels are 3D networked material primarily comprising of hydrophilic polymers which instead of dissolving, absorb a large of water and bio fluids resulting in swelling. Their wide range of customizable biological, physical and chemical characteristics make it an ideal candidate for biomedical purposes. Hydrogel structure is maintained by covalent forces (chemical crosslinking) and inter and intra molecular forces (physical crosslinking). They are classified into synthetic and natural hydrogels, and both have been explored for their usage in tissue engineering field. Natural hydrogels are made up ECM containing polysaccharides and proteins like hyaluronic acid, chitosan and fibrin, collagen respectively. They offer cytocompatibility. Synthetic bio polymers include many compounds of the classes of polyesters, polyamides and polyethylene. For example, PLLA (Poly L-lactic-acid) is an aliphatic polyester and is FDA authorized material which degrades in vivo. [16]

1.5 Polycaprolactone:

PCL is an aliphatic polyester and made up of hexanoate repeating units. The mechanical, thermal, and physical attributes of polycaprolactone are determined by its crystallinity and average molecular weight which also influences its degradability. PCL is a semi crystalline, hydrophobic polymer, has high solubility and low melting point which makes it processing and blending with other polymer materials facile. Its molecular weight varies between 530-630,000 and melting point falls between 59-64 C^o while glass transition temperature is -60 C^o. Owing to its biodegradability, biocompatibility and permeability, it has been thoroughly studied for its application in scaffold material, drug delivery, and drug distribution respectively. It is FDA and CE approved for usage in healthcare and medical fields. Resorption rate of PCL is in order of 3 years which implies that it provides extended support to the damaged tissue until their regeneration is completed.

PCL is mainly synthesized by ring opening polymerization of Ɛ-caprolactone, a cyclic monomer, catalyzed by metal or ions. The monomer is obtained by reaction of hydrogen peroxide with cyclohexanone by Baeyer-Villiger oxidation reaction. Depending upon the type of initiator, its mechanism can be cationic, anionic, and coordination- insertion. Alkoxide is the resulting intermediate in all these mechanisms. Efforts have been made by

researchers to prepare it from MDO (2-methylene-1, 3-dioxepane) and 6-hydroxycaproic acid by radical ROP and condensation respectively[17].

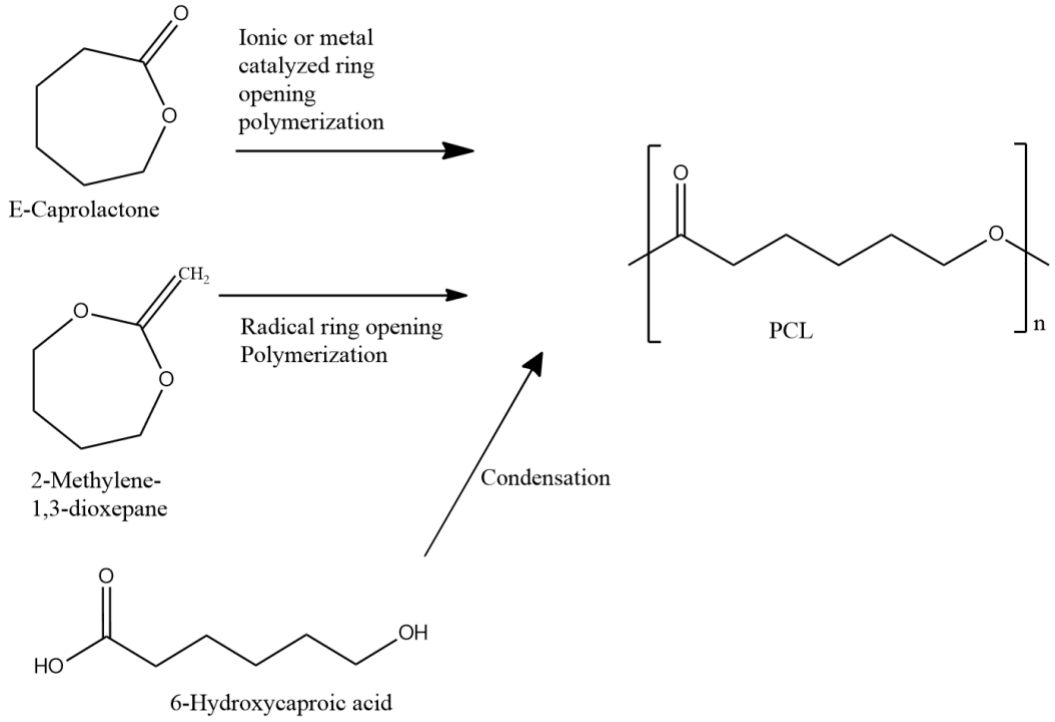

Figure 1.4- Synthesis routes of PCL

Biodegradability of PCL has made it a potential candidate for biomedical applications. Morphology, crystallinity, molecular weight are key factors which determine biodegradability of a material. Amorphous regions degrade earlier than crystalline regions. Biodegradation proceeds by diffusing water into amorphous sites tailed by hydrolytic cleavage of ester bonds catalyzed by carboxylic acid which is formed in situ as a result of hydrolysis. PCL degradation occurs through either surface or bulk erosion conduits. In surface erosion, rate of water permeation is less than the rate of erosion. This kind of pathway is preferred for controlled drug delivery application. Bulk erosion occurs when

rate of water permeation through bulk material is faster than erosion. This kind of pathway is not suitable for drug delivery due to possibility of drug structure destruction.

Cellulose is incorporated into PCL systems to fine tune the rate of biodegradation as per requirement. Amorphous cellulose containing PCL composites undergo degradation way faster than those composites which contain crystalline cellulose fibers, because former have great tendency to absorb water. Soil burial degradation of cellulose incorporated PCL composites was carried out and it was witnessed that 75% degradation occurred with cellulose in comparison to 5% degradation without cellulose in the same time span.

PCL has been used to make artificial construct to stimulate tissue regeneration. Due to slow degradation and efficient mechanical properties, PCL is widely being used for bone tissue engineering. To make it osteoinductive and osteoconductive, PCL is paired with inorganic ceramics such as HA, BCP, β-TCP. PCL-HA and PCL-HA/SP scaffolds were fabricated by 3D plotting system which permits high porosity, excellent mechanical properties and enhanced interconnectivity as compared to the PCL bone substitutes. PCL-HA has better architecture for cell adhesion, cell proliferation and ultimately cell differentiation as consolidated by the MTT and ALP assay. It also helped to foster cellular response and tissue growth by increasing surface area and expanding interconnectivity. Figure 5 (a) and (b) shows that after incorporation of HA, there is gradual increase in the ALP and MTT assay activities of PCL and PCL/SP. [18]

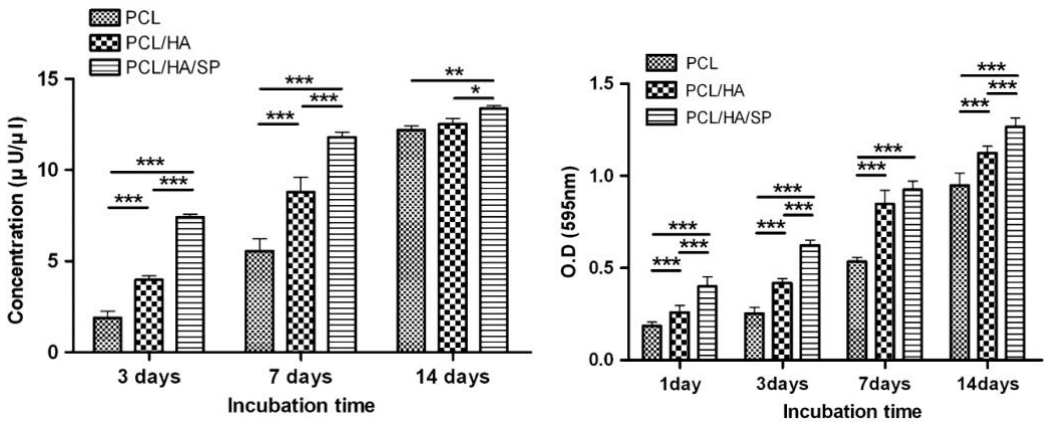

Figure 1.5-(a) ALP activity and (b) MTT assay of MG 63 cell lines

1.6 Cellulose:

Cellulose is one of the most abundent polymer worldwide and is an important structural constituent of green plants' cell wall, oomycetes and algea. This polysaccharide is constituted of hundred to thousand of D-glucose linear chains adjoined through β (1-4) glycosidic linkages. Unlike starch, it is straight chain polysaccharide and due to the equatorial conformation of the glucose moleecules, it assumes rod like conformation. The manifold hydroxyl groups present on the glucose molecules are responsible for holding these chains together and giving mechanical strength to the structure. In addition, hydroxyl groups also confer it hydrophilic character. It is semicrystalline in nature and crystalline to amorphous transition occurs at temprature of 320°C and 25 MPA pressure. Owing to its inexpensive, natural and readily available characteristics, it has attracted much attention in the disciplines of biofeul, drug delivery and composites.

Cellulose is believed to found its potential application in the BTE because of its biocompatible, biochemical and mechanical properties. Bone is predominantly combination of collagen fibers and hydroxyapatite mineral. As cellulose takes after

collagen, supports osteodifferentiation and provide cellular milieu, it can be implicated in the bone implants [19]. Together with HA, cellulose fibers emulate natural bone characteristics like porosity, compressive strength and biocompatiblity but suffer a drwback of collidal stability as HA precipitates. To circumvent this, cellulose oxidation accompained by TEMPO (2, 2, 6, 6-tetramethylpiperidine-1-oxyl) is achieved or any other oxidizing agent is added. The mineralization studies of this bioactive and porous material mimics native bone ECM both chemically and topographically as mesenchymal stem cell differentiate and proliferate towards osteoblasts [20].

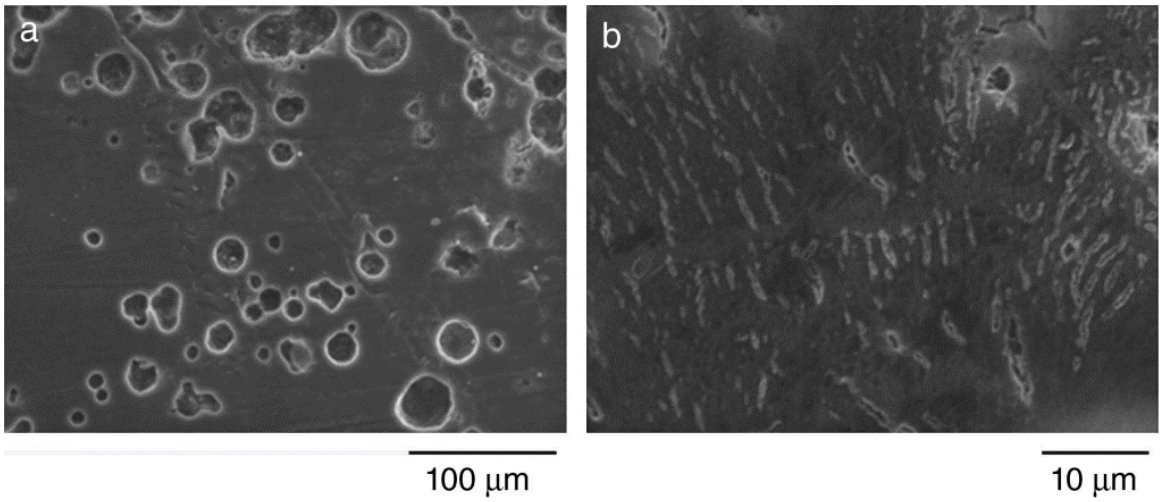

Figure 1.6 SEM microphotographs of cellulose embedded PCL scaffolds

1.7 Bone tissue engineering:

Since the advent of tissue engineering concept, BTE has received huge attention as a new area of promising research. For in contrast to traditional methods of bone repair i.e. autograft and allograft suffer from drawbacks of infection transfer, cost ridden, donor

shortage and immune rejection. The principle of BTE is based on the fact that it utilizes scaffolds or synthetic extracellular matrix along with osteoblast and growth factors to bring about cell recruitment, proliferation and differentiation. Porous scaffolds act as template and facilitate in cell seeding and bone tissue formation. Various materials have been considered and tested for scaffold formation like ceramics, metals and polymers. Due to difficulty in processing and biodegradability, ceramics and metals are ruled out, while polymers make an attractive candidate for bone substitute formation. An enormous growth in the field of polymeric blends is witnessed over the last four decades in terms of their biomedical applications. Bio-artificial blending involves mixing synthetic and natural polymers to impart exceptional mechanical and structural properties to scaffolds/ composites.

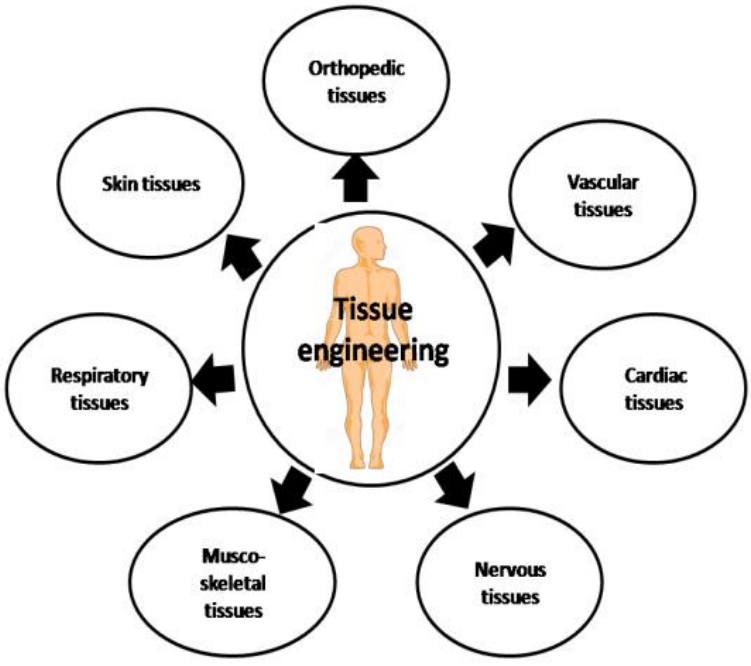

Figure 1.7-Tissue engineering applications

1.7.1 Bone:

Adult Human skeleton is composed of 206 bones giving necessary support and protection to the body organs and help in locomotion. Healthy working of bone is often compromised because of orthopedic problems like bone cysts and tumors, diseases (Osteomyelitis, Osteoporosis, Cancer), revisions of orthopedic implants, spine fusion, and traumatic fractures. To address these bone defects gold standard is bone auto grafts to promote self-healing and regeneration at small scale. Problems like donor site scarcity, pain, hematoma, infection, cost, success rate and need of growing population use of auto graft can't be easily practiced. Other methods like allografts, xenografts have more severe problems like pathogen transmission, and immune rejection.

Bone is an example of heterogeneous material as it is composed of both organic and inorganic phase which constitutes 30% and 70% of the bone individually. The mineral phase is similar to HA, while organic matrix comprises 90% Collagen type-1 and remaining 10% consists of non-collagenous proteins and proteoglycans. When bone is viewed through microscope, three kinds of cells mainly constitute hard tissue which are named as osteocytes, osteoblasts and osteoclasts where osteoblast is concerned with the bone formation and mineralization and osteocyte are the osteoblasts which have been trapped in the intercellular matrix whereas, osteoclast is responsible for the bone degradation by direct enzymatic or chemical invasion bone cells [21]. Bone serves as the storehouse of calcium and magnesium.

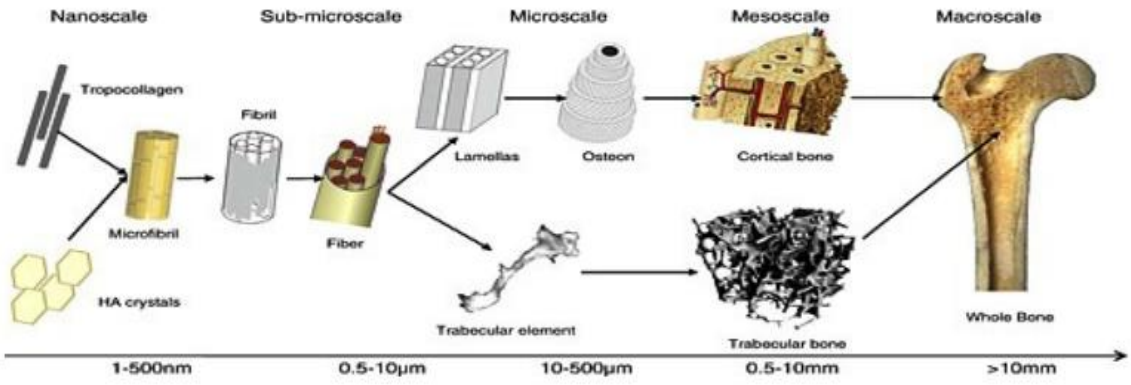

Figure 1.8 Bone anatomy at different scale lengths

1.7.2 Whitlockite:

Whitlockite (WH, $Ca_{18}Mg_2(HPO_4)_2(PO_4)_{12}$) is the most abundant inorganic phase in the bone besides HAP. It occupies 20-35% weight of the bone and unlike HAP, it has high stability in the acidic bone regeneration environment and is found in the form of molecular clusters. In contrast to HA, it shows increased solubility due to its ion releasing capacity. [22]

WH emulates natural bone remodeling process by performing three fundamental functions: it inhibits monocyte's differentiation into osteoclasts thus, preventing osteoclastic activity, it regulates osteogenic differentiation and also transforms into HAP through concurrent supply of Mg2+ and PO4− ions. Osteogenic differentiation is induced by absorption of PO4− and Mg2+ ions by SLC20a1 and Magt1 protein channels of hTMSCs respectively as these transporter ions lead to enhanced osteogenesis by stimulating ERK pathway of stem cells. Through phase transformation, WH stimulates enhanced bone cell's proliferation and gene expression for mineralization.[23]

Besides, WH offers improved protein absorption due to development of electrostatic attraction between negatively charged WH surface and positively charged proteins. Negatively charged surface of WH leads to reduction in surrounding's pH which causes ionization of the osteogenic proteins.[24]Due to synergistic effect of both HA and WH, biphasic composite exhibit improved bone regeneration activity than monophasic material as HA offers mechanical strength and WH extends improved osteogenic activity. Optimal ratio between HA and WH for maximum osteogenic differentiation is 3:1 which is similar to natural bone. [25] Structure rationale suggests that TCP, a synthetic analogue of WH, first transforms to TCMP with the incorporation of Mg^{2+} at Ca5 and Ca4 positions and later with the addition of HPO_4^{2-} phase changes to WH. Though TCP and WH have similar XRD patterns and anion to cation ratio, they can be distinguished by HPO_4^{2-} presence shown in FTIR and stability region of their phases. Unlike TCP, WH contains both HPO_4^{2} and $PO4^{3-}$ and is stable under biological conditions. Previously, WH has been prepared by drop wise mixing of Ca^{2+}, Mg^{2+} ions into phosphate containing solution or WH obtained from aqueous solution by mixing calcium, magnesium and phosphate containing salts in water at 100 ^{o}C. Recently, WH is prepared by precipitation reaction of ternary aqueous system containing $Ca(OH)_2$, $Mg(OH)_2$ and H_3PO4. [26]

1.7.3 Hydroxyapaptite:

Hydroxyapaptite is the most abundant inorganic phase in the hard tissue. Its general formula is Ca_{10} $(OH)_2(PO4)_6$. It is only calcium phosphate compound which is thermodynamically stable at neutral pH. It is nonstoichiometric material and due to its flexible crystal lattice, it can accept atomic disorders. In comparison to the natural tissue regeneration frequency, HAP's resorption rate is much lower due to less solubility.[27]

HA phase transforms to WH phase through five intermediate steps. In stage I, H_3PO4 reacts with $Ca(OH)_2$ to produce HAP. While at stage II, magnesium phosphate (MP) is generated by reaction between $Mg(OH)_2$ and H_3PO_4. The newly synthesized HAP converted to dicalcium phosphate dehydrate (DCPD) in acidic environment. At stage IV, MP, HAP and DCPD began to dissolve to form rhombohedral WH resultantly in pure phase. [22]

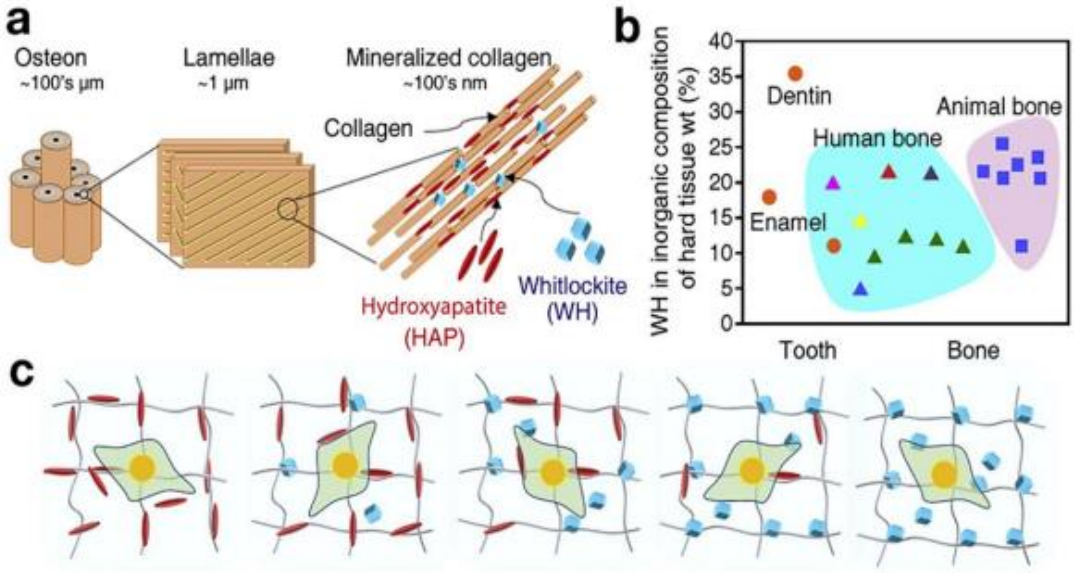

Figure 1.9 (a) structure and composition of bone from micro to nano level (b) amount of WH in the human and animals is shown which is calculated by measuring Mg present in the bone (c) schematic representation of osteogenic differentiation of human mesenchymal cells with different contents of WH and HA.

HAP has been extensively used for tissue engineering and controlled drug release applications due to its superior biodegradability, biocompatibility, osteoinductive and osteoconductive abilities. But aggregation, less flexibility, difficulty in dispersion and

brittleness make it a challenging ceramic material. The word “apatite” was first time used in 1788 refers to the similar compound, having variable composition. It has hexagonal rhombic shape and lattice parameters ‘a’ and ‘c’ have 0.95nm and 0.69nm values. Unlike whitlockite, HA lab synthesis is facile and can be prepared from a variety of methods and precursors. Kamitakahara et al. synthesized HA hydrothermally by treating octacalcium phosphate (OCP) powder with distilled water for 24hrs and discovered that hydrothermal conditions can control crystal growth of HA. Previously, alpha-tricalcium phosphate hydrothermal transformation lead to the formation of HA. In bone nano crystalline HA is dispersed in collagen matrix making bone a true nanocomposite and unlike microcrystalline HA, nanocrystalline HA offers excellent cell proliferation, differentiation and adhesion.[28]

Chapter 2

2 Literature Review:

2.1 Hydroxyapatite:

In 2018, Chang et al. investigated the synergistic effect of HAP and WH by fabricating hydrogel scaffolds because both HAP and WH when combined offer improved bio and osteogenic activity than in their monophase. In addition, to find out the optimal compositional ratio between HAP and WH, they prepared nanocomposite hydrogel scaffolds for the growth of mesenchymal stem cells in various ratios and observed that 3-1 ratio is the optimum composition for osteogenic gene expression and is similar to human bone material [29].

In 2016, a study was carried out by Jang et al. to make a comparison among β-tricalcium phosphate, hydroxyapatite, and whitlockite in terms of usage as bio ceramic material. It was reported that whitlockite, which is secondary inorganic phase in the bone tissue, showed better osteogenic regeneration and differentiation in vivo and in vitro testing as compared to HAP and β-TCP. WH scaffolds have similar chemical structure as natural human bone and comparable resorbability [30].

In 2020, Yu et al. determined that poly ether-ether-ketone (PEEK) composites with Nano-hydroxyapatite (n-HAP) offer enhanced mechanical strength and bio-interfacial attraction, then alone usage of PEEK in hard tissue repair. Varied concentration of nHAP showed different extent of the afore mentioned properties, but it was observed that 30% and 10%

addition of nHAP exhibited optimal interfacial affinity and compact strength respectively by increasing interaction and adhesion between polymer, nHAP and surrounding muscles. The results are consolidated by the in-vivo and in-vitro studies [31].

In August 2020, Cakmak et al. fabricated bone implants of four composites namely polycaprolactone (PCL), bacterial cellulose (BC), gelatin (GEL), hydroxyapatite (HA), by varying anvil rates from twenty to eighty percent, using 3D printing method. All scaffolds prepared with 80% anvil rate have both optimal porosity and uniformity rate. PCL/GEL/BC scaffolds presented prime tensile strength and good cell adhesion and cell viability were demonstrated by PCL/GEL/BC/0.25% HA [32].

Nyberg et al. in 2017 manufactured 3D printing porous bone implants of PCL using fused deposition modeling and later functionalized these scaffolds with HA, tri calcium phosphate, decellularized bone matrix and Bio Oss. Print quality was assessed and it was found that PCL/HA and PCL print quality was higher (0.8) than other composites (0.7). Incorporation of mineral additives caused increase in the osteo inductiveness in PCL/TCP and PCL/HA which was attributed to the presence of collagen phase or apatite structure. While PCL/BO and PCL/DCB showed improved deposition of minerals and collagen up regulation. It was concluded that 3D printed PCL scaffolds doped with DCB and BO are better contender for the bone healing scaffolds than other composites [33].

Jing et al. prepared 3D PCL bone substitutes via methods of gas foaming and co-extrusion method. In order to make these blends mechanically strong and biologically more active, HA and HNT were added as filler and their influence on the mechanical, morphological and rheological properties were compared. Due to the unusual structure of HNT, onset of decomposition temperature is reduced thus affecting thermal stability of composite blends.

In the same way, compressive moduli of the HNT containing scaffolds was higher than those of containing HA due to greater surface to volume ratio. Biological studies were investigated by using hMCs as cell model and maximum cell proliferation and cell differentiation was observed with 5% HA and 1% HNT [34].

Yan et al. studied the effect of n-HA on the PLA (poly lactic acid)/ PBAT (poly butylene adipate-Co-terephthalate) modified with microcrystalline cellulose. N-HA was added as a nucleating agent and increase the crystallinity substantially, while MCC facilitates degradation. Principle of solution blending was applied to synthesize these composites. SEM and TEM results depicted that uniform distribution of n-HA was observed till the 6% w/w ratio of the biomaterial, while agglomeration started when addition exceeds 10%. Addition of PBAT in the PLA matrices reduced its crystallinity but increased biocombatility toughness, and sea –island structures. N-HA induced the production of native bone structure [35].

Chen and Sun in 2005 produced HA reinforced PCL blends via melt blending method. DMTA (dynamic mechanical thermal analysis) and DSC (differential scanning calorimetery) results indicated that there was an increase in the crystallization, glass transition and melting temperature with the incorporation of HA due to nucleation and facilitation in crystallization. Quasi-static testing showed that both Young's and storage moduli was improved, and ductility was introduced in the binary composites. Improvement in the viscosity and elasticity, studied by latest rheometric expansion system, witnessed due to the presence of reinforcement material [36].

Salerno et al. prepared PCL and PCL/nHA biodegradable bone scaffolds by combining NaCl reverse template and gas foaming techniques. Gas foaming pressure induced

nucleation and pore formation with in polymeric phase, whereas reverse templating lead to the formation of multi-scaled pores of various sizes whose relation was studied with NaCl which was added in the range of 85-95 %. The outcomes suggested that to draw a link between elastic properties of PCL and hybrid PCL blends. In vitro analysis was performed on pre-osteoblast MG63 cell lines to assess biocompatibility. TGA results confirmed that incorporation of HA in 5-20% range increased degradation temperature [37].

Park et al. adopted rapid prototyping technique for the production of PCL, PCL/HA and PCL/HA/SP porous scaffolds with good interconnectedness and excellent mechanical attributes. This 3D plotting technique gives control of pore size and permits stretchy tissue design. Cell adhesion was studied by seeding these bone composites on MG 63 cells. Scaffolds with shifted patterns had better cell adhesion than those without shifted pattern had higher compressive module. Alkaline phosphatase analysis and MTT assay demonstrated that cell differentiation and proliferation was also observed highest with PCL/HA/SP composition [38].

2.2 PCL:

Chuenjitkuntawor et al. in 2009 developed PCL scaffolds incorporated with HA by applying combination of particulate leaching and solvent casting techniques. As the pore size and density of the scaffolds was dependent on the concentration of porogen, so 1:10 PCL to porogen ratio was selected for further studies and pore size of 400-500 μm was obtained. The addition of HA caused an increase in the density, porosity and maximum compressive rigidity of the product was obtained with 40% w/w HA. In vivo carried on mouse calvarial model and in vitro analysis demonstrated that PCL/HA supplementary osteogenic differentiation than with alone PCL [39].

Biscaia et al explored the use of ES as bio filler with polymer for application in tissue engineering field. PCL and PCL/ES (eggshell) 3D scaffolds were prepared by additive manufacturing and melt blending techniques respectively. Thermogravimetric Analysis and Differential Scanning Calorimetry investigation showed that addition of ES had positive impact on the thermal stability and crystallization of the scaffolds. FTIR and XRD showed characteristic bands and peaks respectively of calcium carbonate and no chemical modification was observed [40].

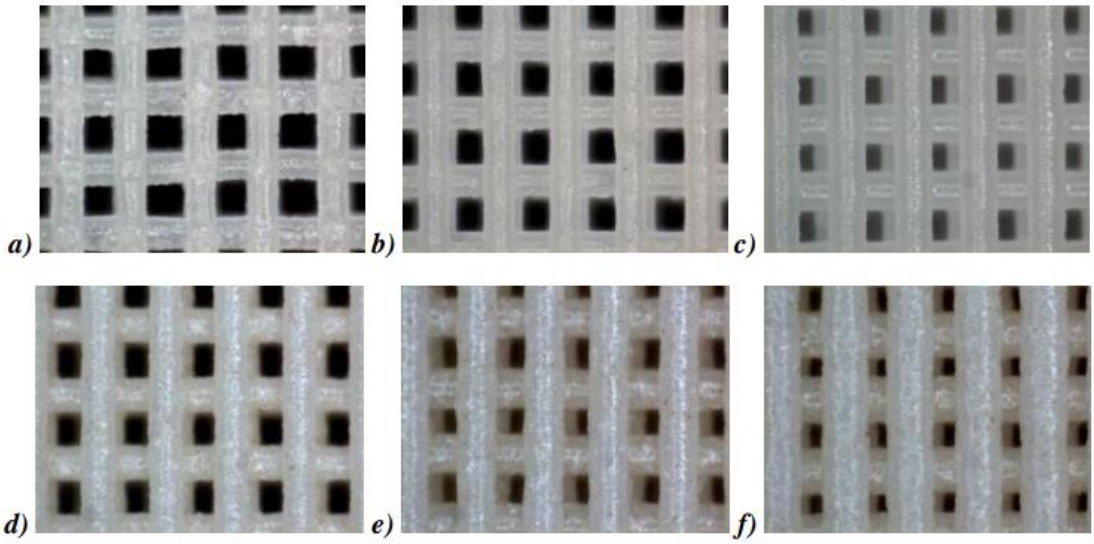

Figure 2.1- Stereoscopic imageries of PCL-ES scaffolds at diverse values of screw rotation velocity

In April 2007, Catledge et al. electro spun triphasic scaffolds of HA, collagen type-1 and PCL in the ratio of 20/30/50 respectively, followed by their characterization for HA particles dispersion, nan indentation, chemical composition and fiber morphology. SEM demonstrated that average diameter of these fibers matches with the natural bone matrix whose value is 180±50 nm, while confocal microscopy proved the uniform distribution of

HA particles with minute agglomeration. These triphasic fibers were compared with pure collagen, pure PCL, HA/PCL (20/80) and HA/collagen (20/80) for mechanical strength and it showed decreasing modulus in the following order: collagen/nano-HA> triphasic > collagen> PCL/nano-HA> PCL [41].

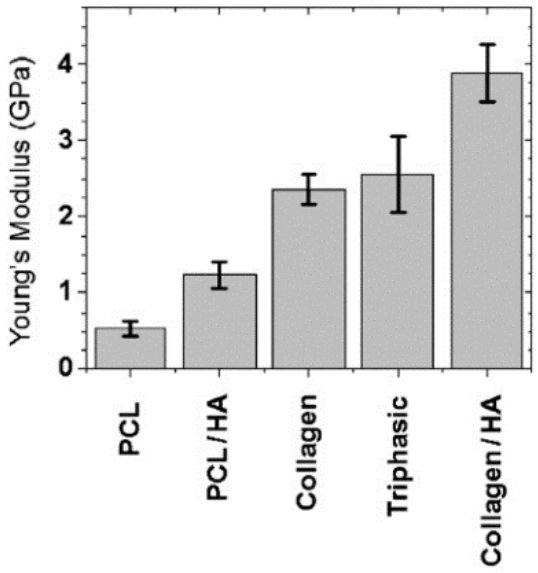

Figure 2.2- Measured Young's modulus values of scaffolds through nanoidentation

To overcome the difficulty in mimicking the structure and role of natural organs, Gómez-Lizárraga et al. prepared 3D scaffolds of PCL and PCL-composite using HA and Nukbone as ceramic material in 20%, 10%, and 5% by applying bioplotting which is a RP technique. By carefully applying optimal parameter combinations, 323 μm pore size is obtained which is adequate for mechanically stable bone growth. Mechanical studies exhibited that the Young's modulus in the range of 0.121-0.171 GPa which coincides with the native bone. FTIR spectrum of composite scaffolds confirmed the presence of carbonyl and phosphate bands, in addition to amide band in case of Nukbone which indicated the presence of 24%

collagen. The comparative study assessed that PCL/NKB is a better candidate for osteogenic application than PCL/HA [42].

To investigate the interaction of PCL/ HA nanocomposites with human mesenchymal cells for growth, adhesion, and bone differentiation, Totaro et al. in 2015 designed micro scaffolds of PCL and HA from a versatile method of phase separation. The results obtained by in vitro explores that the PCL/30HA induces cell growth without adding osteo cells growth factors. These micro scaffolds act as a site of attachment, osteocellular differentiation, and osteogenic lineage developed due to the presence of HA, in addition to development of precursors of bone tissue. These results are consolidated by histological analysis, alizarin red analysis, and calcium deposition assay [43].

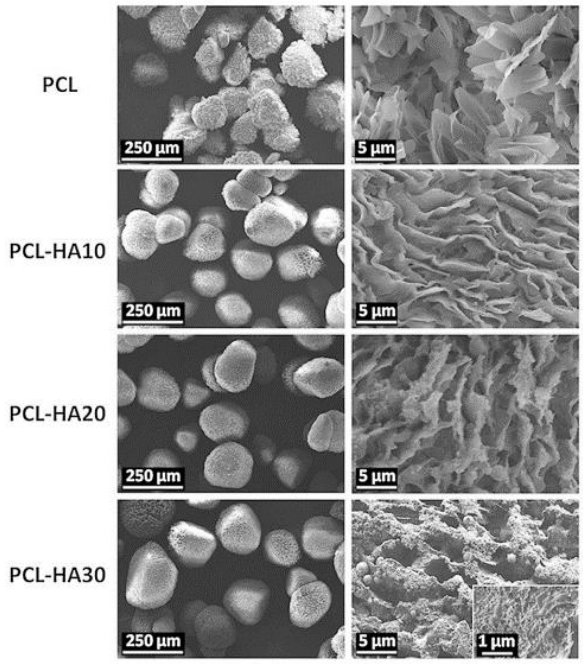

Figure 2.3- SEM pictures of neat PCL and HA incorporated PCL showing their morphology.

Wutticharoenmongkol et al. prepared PCL bone scaffoldings by elctrospinning method incorporated with calcium carbonate and HA particles and investigated its potential use in osteocyte regeneration for proliferation, alkaline phosphatase and attachment activity, with SaOS2 (human osteoblasts) cells which were cultured on these blends for in vitro study. The corresponding results were compared with the solution casting blends and tissue-culture polystyrene plate methods. It was found that electrospun films showed much better proliferation, adhesion and ALP activity. Scaffold containing 1% HA showed maximum ALP activity. Mechanical testing of the blends confirmed the higher efficiency of electro spun blends [44].

In 2013, Sousa et al., prepared surface modified PCL matrices for its usage in the tissue engineering domain to provide biological and physiological environment required for tissue adhesion, provision of necessary growth nutrients and minerals as well as proliferation. Due to the hydrophobic nature of this biomaterial, cell adhesion is challenging, so to overcome these matrices were activated with a coating of collagen which is hydrophilic. Thus, it facilitates in the osteocyte adhesion corroborated by cell culture studies [45].

Domınguez et al. in 2018 proposed to add microcrystalline cellulose as a filler in the polycaprolactone matrices to fabricate three dimensional scaffolds in order to improve its biological and mechanical properties for their potential application in the field of tissue engineering. MCC was added in the 2, 5, 10 % of w/w and results were compared with the pure PCL blends. These scaffolds were made by fused deposition modelling. TGA, proliferation and mechanical assay revealed that blends containing 2-5 % w/w

concentration of MCC were suitable for usage in biomedical domain. The porosity value was determined to be 50-60 %, while the pore size was 450-500 nm [46].

In 2014 Qian et al. probed the effect of gelatin- chitosan complex as an additive on the PCL blends. Elctrospinning technique was adopted to make nano fibrous scaffolds whose fibers' diameter was smaller than pristine PCL as indicated by SEM and average diameter was smallest when the 25/75 w/w ratio of CS to PCL . X-ray results revealed that with the gradual addition of GC gel due to amorphous nature of GC gel, while the hydrophilicity was increased owing to the presence of amine and carboxyl groups. Cell viability and proliferation was tested by porcine iliac endothelial cells and CS-PCL showed better bio compatibility [47].

In 2000, a new kind of rapid prototyping method, fused deposition modelling was adopted by Hutmacher et al. to design and synthesize 3D scaffolds of PCL. This method allows increased interconnectivity, high reproducibility and ease to control design. The honey comb structure had 61% porosity and pore size was in the range of 620micro meter. Compressive stiffness of two scaffold architecture was determined and it was assumed that three angle matrices had decreased stiffness than five angle matrices. In vitro studies were conducted on human periosteal and fibroblasts cells. These cells showed extracellular matrix generation and cell growth in a period of 3-4 weeks producing a highly interconnected polycaprolactone matrix [48].

Sani et al. engineered bone scaffolds based on the graft copolymerization of PCL and chitosan, so the resultant blends mimic the native bone morphology and physiology. Electro spinning method was adopted to make nano fibrous matrixes by placing PCL monomers onto the hydroxyl group of chitosan and HA nanoparticles were incorporated

into them. A substantial decrease in the diameter and diametric distribution of PCL fibers was observed with the addition of chitosan. In contrast to chitosan, nHA increased the fiber diameter along with reduction in porosity. Cell viability test on NIH-3T3 consolidated the idea of nanofibrous biomimetic scaffolds being bioactive and cytocombatible [49].

Yang Mi et al. produced PCL matrixes incorporated with varying amount of CNC (cellulose nanocrystals) by twin screw extrusion method. Microcellular injection molding procedure was followed to foam these nano composites using CO_2 as blowing agent. CNCs acted as nucleating agents and lead to greater pore density and smaller pore size. Due to reinforcement effect of CNC, increase in its amount lead to increased storage and tensile moduli, complex viscosities in both foamed and solid composites but significant improvement was seen in foamed composites due to its porous structure. Cell culture studies with 3T3 fibroblast reveals that 0.5-1% content on CNC is suitable for the cell viability, while crystallinity and glass transition temperature was highest for 5% CNC mass [50].

In 2017 Abuelreich et al. investigated the properties of chitosan reinforced PCL nano fibrous scaffolds for their usage in bone tissue engineering. For this purpose, they grew osteoblast and chondrocyte of human mesenchymal cells, 50000 cells at each piece of these scaffolds. Cell proliferation and viability were tested by Blue Alarmar staining. It testified that CS/PCL scaffold induce and support proliferation either differentiation occur or not. SEM was carried out to determine cells differentiation and attachment. It was discovered that rate of proliferation was high for the cells which differentiates into chondrocytes showing gene expression for COMP, COLLAGEN-II and SOX9 than for those which grow into osteoblasts [51].

Assunta Basile and coworkers realized microporous membranes of functionalized PCL/MAGMA and PCL/DMAEA with HA nano-whiskers incorporation by applying solvent- nonsolvent technique of phase inversion. Although PCL/MAGMA showed dense structure, but it has superior degradation, water uptake and differentiation rate than PCL/DMAEA which entails porous architecture and is more promising in terms of cellular growth and proliferation. Collectively, these nano-porous membranes stimulate effective bone regeneration as porous side offers site for cell attachment and spread,s whereas dense side protects damages site from invasion of epithelial cells, making them a potential contender for the treatment of periodontal diseases [52].

2.3 Whitlockite:

In order to understand the bone remodeling procedure and to elucidate complex signal paths between extracellular bone materials, whitlockite role can be discerned as bone renovating procedure consists of compound signaling ways among osteoclasts, control mechanism and osteoblast to get a balanced homeostasis of proliferation.

Hwan D. Kim et al. demonstrated that whitlockite is a synthetic inorganic compound that stimulates osteogenic growth and inhibits osteoclastic performance to recapitulate early bone regeneration by converting itself into hydroxyapatite which is mechanically stronger than WH. Tis transformation occurs due to incessant supply of Mg^{2+} and PO_4^{3+} under biological environment. Based on structural studies, this dynamic phase conversion of WH into HA is attributed as the prime factor in denser structure of neo bone regeneration. This research bursts the previous concepts of bone mineralization and puts forward idea of self-healing property of these minerals [53].

To investigate the effect of Mg content on the morphological and compositional properties of HAP and WH matrices, Baue et al. in 2020 synthesized calcium phosphate scaffolds by applying hydrothermal method and using cuttlefish bone skeletons, magnesium perchlorate, ammonium dihydrogen phosphate and magnesium chloride hexahydrate as reagents. Structural analysis revealed that Mg preferably incorporated into WH phase and increased the tensile and compression strength of WH matrices. Histochemical assay exhibited that WH/ HAP in ratio of 10/90 and 30/70 containing CaP/Mg showed better osteocalcein and collagen [54].

With the aim to manufacture mechanically strong and bioactive bone substitute material, Huang and his coworkers fabricated PCL/ TCP hybrid bio composites by adding TCP in different weight ratios and these bio composites were analyzed for biological and physical properties. With the increase in TCP incorporation, enhancement in the setting time and injectibility was seen. Due to lower contact angle with TCP containing composites, optimal cell adhesion, proliferation and differentiation were observed with 50% w/w TCP containing composites. ALP assay performed on human bone mesenchymal cells (hBMCS) and higher ALP enzyme activity was observed with TCP50 [55].

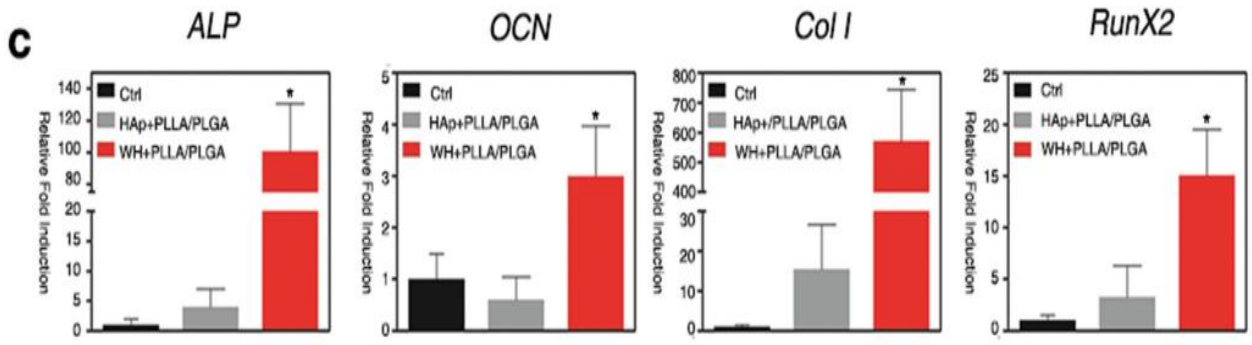

Figure 2.4- Osteogenic gene expression of HA and WH based PLLA/PLGA composites

Yang et al. fabricated reduced graphene oxide (RGO) reinforced Zn metal scaffolds via laser powder bed fusion (LPBF), to investigate the effect of RGO on the Zn based bone implant material. It was found that due to homogeneous distribution of RGO, grain refinement was induced which in tandem with higher load transfer capacity of RGO enhanced ductility and mechanical strength of zinc. Presence of oxygen containing groups on the surface of RGO lead to the cell growth, differentiation and cell functioning [56].

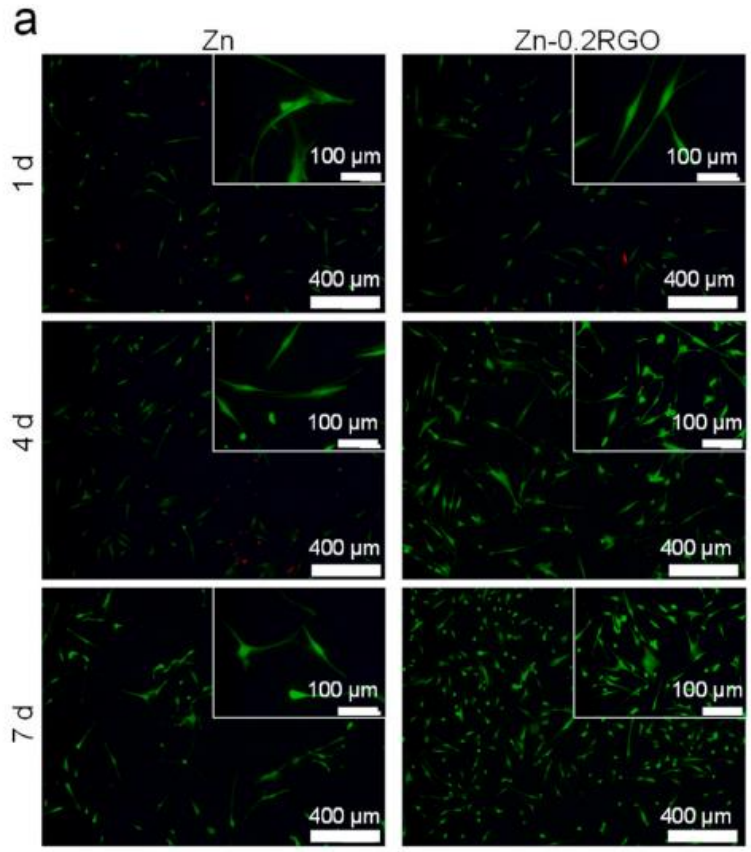

Figure 2.5-LIVE/DEAD assay's fluorescent images

Arrieta et al. in 2020 fabricated PCL mats incorporated with MCC and PHB (ploy 3-hydroxybutyrate) by electro spinning method. First neat PCL, PCL/PHB and PCL/MCC mats were prepared in different concentrations and then conditions were optimized to acquire scalable PCL mats. TGA graphs represented that addition of fillers lead to reduction in the thermal stability of PCL matrix and SEM showed that formation of beads was reduced due to PHB incorporation. It was observed by mechanical studies that flexibility of bulk PCL was greater than electro spin PCL which was tailored by PHB integration, so these composites can be used for biomedical, packaging and industrial application [57].

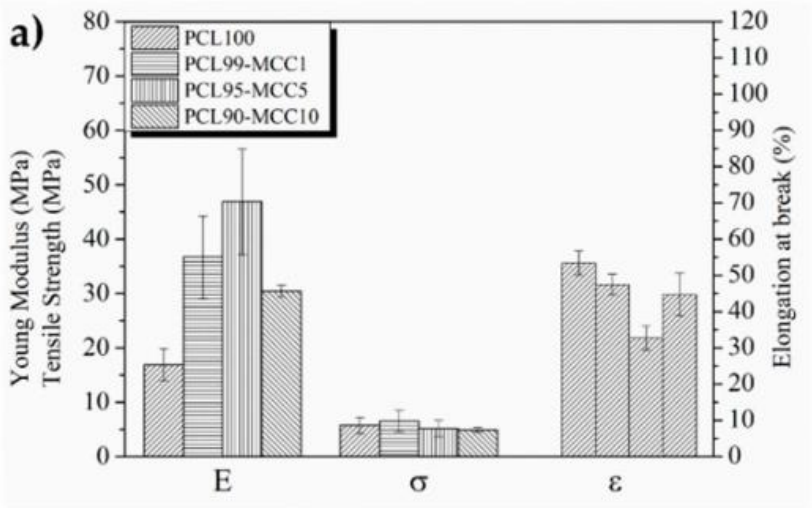

Figure 2.6- Graphical representation of mechanical strength of neat PCL and MCC based bone composites

In year 2020, a biomaterial formulation based on collagen, polyurethane and cellulose was obtained by Spiridon et al. through dissolving in butyl methylimidazole chloride solvent. To this matrix lipoic acid and tannin were added as filler to enhance compressive moduli and bioavailability of active elements which were improved up to 139kPa and 30% respectively. Addition of bioactive material also lead to an increase in the antioxidant property as compare to the base matrix by 50%. An increment in the mucoadhesiveness was also seen due to presence of thiol groups which forms disulfide bonds. SEM studies witnessed formation of H-bonding between filler and base matrix [58].

A multi constituent polymer blend containing PLA, MCC and PBS was prepared by Rasheed et al. by adopting melt blending and hot pressing techniques. MCC was used reinforcement material and caused an increase in the thermal stability up to its 1% content due to uniform dispersal in the matrix. On the addition of PBS, reduction in tensile strength

was observed in contrast to MCC incorporation which lead to increase in the mechanical strength attributed to the restricted molecules movement which caused stiffness. However, elongation at break point was higher for the PBS containing blends in comparison to MCC containing blends. MCC incorporation also caused decline in brittleness while PBS enhanced PLA's flexibility [59].

Bone substitute composites of Octacalcium phosphate (OCP) and PCL were synthesized by Heydari and coworkers through electrospinning method in 0,5,10 % proportions of OCP. The introduction of OCP caused fiber thickness lessening corroborated by SEM analysis and significantly improved mechanical strength indicators such as tensile strain, Young Modulus. Cell viability was determined through MTT assay on human osteoblast G-292 cells for `1, 3, and 5 days. OCP containing composites induces greater cell production and proliferation. When these scaffolds were immersed in SBF solution, it lead to formation of hydroxyapatite layer on its exterior surface [60].

Chapter 3

3 Materials and Methods:

3.1 Materials:

PCL (number average Molecular weight 70,000g/mol) was acquired from Polyscience Inc. (USA). Sample was small pellets and appeared white. Microcrystalline Cellulose (MCC) (DAEJUNG 20–100 um), Chloroform research grade (99%pure) was purchased from sigma Aldrich Co., USA. Calcium nitrate tetrahydrate $Ca(NO_3)_2 \cdot 4H_2O$ reagent grade ACS molecular weight 236.15g/mol assay (complexometric assay 99 - 103 %), Di-Ammonium hydrogen phosphate, $(NH_4)_2HPO_4$, reagent grade, ACS molecular weight132.06 g/mol (98 %), Calcium hydroxide $Ca(OH)_2$, Magnesium hydroxide $Mg(OH)_2$ Ammonia Solution 35% NH_3 sol, Certified AR for Analysis, d=0.88, Fisher Chemicals, Phosphoric Acid (H3PO4) and Deionized water were acquired and used as such.

3.2 Synthesis of the Hydroxyapatite nanoparticles:

Hydroxyapatite nanoparticles (nHA) synthesis was carried out by combining calcium (calcium nitrate tetrahydrate ($Ca(NO_3)_2.4H_2O$)) and phosphorus (diammonium hydrogen phosphate ($(NH_4)_2HPO_4$)) sources by maintaining pH 12 using NH_3 sol [61]. Briefly, aqueous solutions of $Ca(NO_3)_2.4H_2O$ (dissolving 32.8125 g in 200 mL deionized water at 80 ^oC) and $(NH_4)_2HPO_4$) (9.5 g in 137.5mL in deionized water at 80^oC) were prepared on a magnetic hot plate. Two solutions were mixed by drop wise addition of $Ca(NO_3)_2.4H_2O$ solution into highly basic $(NH_4)_2HPO_4$) solution for 2 hours at 80^oC, followed by 24 hours

for aging. After aging nHA precipitates were filtered and washed with deionized water. Residue nHA was vacuum oven dried at 80 ^{o}C for 24 hours. Muffle furnace was used for calcination at 500^{o}C for 2 hours. Chemical reaction for the synthesis of nHA is described in the Equation 1:

$$Ca(NO_3)_2\ 4H_2O + 6(NH_4)_2HPO_4 + 8NH_4OH \longrightarrow Ca(PO_4)_6(OH)_2 + 20NH_4NO_3 + 46H_2O$$

Eq-1

3.3 Synthesis of the Whitlockite nanoparticles:

Whitlockite are synthesized by previously reported wet chemical precipitation method [23, 62, 63] , in which Ca (OH) $_2$ and Mg (OH)$_2$ were taken as preliminary reagents. Initially, 0.37M of Ca (OH) $_2$ and o.13M Mg (OH) $_2$ solutions were prepared in distilled water. Then, equal proportions of Ca (OH) $_2$ and Mg (OH) $_2$ were mixed in distilled water by keeping the temperature of the system below boiling water. Whereas a suitable quantity of 0.5M H_3PO_4 was added, in a drop wise manner, into the Ca (OH)$_2$ - Mg(OH) solution at the speed of 12.5 mL min $^{-1}$ along with continuously stirring. The resulting precipitates were aged for 24 hours to obtain particles of sufficient size and then assembled using a filter press. The sample was calcined at appropriate temperature for sufficient time to remove any volatile impurities.

3.4 Synthesis of PCL-cellulose films:

Four PCL-cellulose composite systems were prepared by solvent casting method, containing 100% (w/w) – 0%, 95%-5%, 90%-10%, 85%-15% of PCL-Cellulose respectively. For first system, 1g PCL pellets were accurately weighed in a reagent bottle and homogenously dissolved in 20mL of chloroform using magnetic stirrer at 50 C^{o} for 2 hours. Later, this homogenous viscous solution was poured into petri dish and placed at

room temperature for 24 hours to let the solvent evaporate. For PCL/MCC composite preparation, 0.95g, 0.90g, 0.85g of PCL granules were dissolved in 15mL of chloroform separately in 3 different reagent bottles with the help of magnetic shaker keeping temperature at 50 Cº. In order to disperse powdered MCC in chloroform solvent, 0.05g, 0.10g and 0.15g of MCC is dispersed into 5mL of chloroform separately in different beakers and then poured into PCL solutions respectively and stirred for 2 hours. Then these viscous fluids were deposited in petri dishes and dried at room temperature for 24 hours, so no solvent was left behind.

3.5 Synthesis of PCL-cellulose films with nHA and nWH:

Based on the mechanical results of the aforementioned composites, 95%-5% PCL/ MCC composite was selected for further analysis. For this purpose, three different composites with three varying amounts (1%, 5%, 10% w/w) of WH and HA were fabricated separately. First in three different reagent bottles 0.95g of PCL pellets were dissolved in 15mL of chloroform separately by stirring magnetically for 2 hours on a hot plate at 50 Cº. 0.05g of MCC was dispersed in 5mL of chloroform with the help of magnetic stirrer at 50 Cº in three different beakers separately for 1 hour. To make solutions homogeneous, MCC solutions were poured into PCL solutions and stirred for 1 hour. Then 0.01g, 0.05g and 0.10g of nWH were rightly weighted and dissolved into 5ml of chloroform in three different beakers at room temperature for 1 hour. These nWH solutions were added to the PCL-MCC solution and magnetically stirred for 2 hours and to get the solvent evaporated, solutions were poured into petri dishes and left for 24 hours. Same procedure was repeated with nHA to get its composites of 1%, 5%, 10% w/w concentration.

Table 2.1 Representing composition of PCL/MCC blends and PC5/nHA and PC5/nWH Compositions.

Polymer System	Sample Code	Weight of PCL(g)	Weight of MCC(g)	Weight of nHA(g) /nWH
PCL	PC	1.00	-	-
PCL/MCC-5%	PC5	0.95	0.05	-
PCL/MCC-10%	PC10	0.90	0.10	-
PCL/MCC-15%	PC15	0.85	0.15	-
PCL/MCC-5%-nHA1%	PC5-HA1	0.95	0.05	0.01
PCL/MCC-5%-nHA5	PC5-HA5	0.95	0.05	0.05
PCL/MCC-5%-nHA10%	PC5-HA10	0.95	0.05	0.10
PCL/MCC-5%-nWH1%	PC5-WH1	0.95	0.05	0.01
PCL/MCC-5%-nWH5%	PC5-WH5	0.95	0.05	0.05
PCL/MCC-5%-nWH10%	PC5-WH10	0.95	0.05	0.10

3.6 Characterization Techniques:

To confirm the crystal structure and homogeneity of HA and WH Powder XRD was performed by (model: DRON8, country: Russia), voltage 40kv and current 20 mA. For average crystallite size was calculated by using Scherer's formula considering Bragg's peaks (211) and (310) $D = k\lambda/\beta\cos(\Theta)$Where D represents crystal size, k=shape factor (0.008), λ= incident wavelength, β=broadening of peak at half of the maximum peak, Θ is diffraction angle. WAXD of PCL/Cellulose, PCL/Cellulose/nWH, and PCL/Cellulose/nHA were recorded at a rate of 2° per min varying 2Θ 5°-90° at room temperature. Step size for each measurement was 0.04 and count time per step was 1 sec per step.

FTIR spectra of samples were recorded on Bruker PLATINUM ATR and vertex 70 FT-IR spectrophotometer over an observation range of 500-4000 cm^{-1}. Dried thin films of the PCL/Cellulose, PCL/Cellulose/nWH, and PCL/Cellulose/nHA were placed to get IR data.

Samples were subjected to thermo gravimetric analysis by carrying out a heating cycle upto 800^{o}C with a heating rate of 10^{o}C/min with a gas flow of 50ml/min in each case. The heating range was from 25 ^{o}C to 800^{o}C under inert nitrogen atmosphere.

Differential scanning calorimetry was performed on DSC 250 under nitrogen gas atmosphere of 20mL/min. Each sample of 7mg was weighed and placed in Tzero Aluminum pan. Each sample was first heated to 100 ^{o}C then cooled to -10 ^{o}C and then again heated to 100 ^{o}C. The degree of crystallinity (χ_c) and melting temperature (T_m) was measured through following equation:

$$Xc = 100\% \times [\Delta H_m / \Delta H_{cm}] \times 1/W_{PCL}$$

Where ΔH_{cm} is the melting enthalpy of pure PCL and ΔH_m is the melting enthalpy of samples.

Morphological analysis of the samples was obtained by using JEOL JSM-6490A. Nanoparticle morphology and size was observed by placing powder sample on carbon tape and then directly gold sputtering the powdered nanoparticles. Nanoparticles were also suspended in deionized water and then after water evaporation sample was gold sputter coated for SEM analysis. Cryofractured morphology of pure polymer films, blend films and nanocomposites films at room temperatures. Fresh Cryofractured surface was produced by dipping the samples in liquid Nitrogen and then breaking these cold samples. Samples were fixed with the Aluminum stub with the help of double-sided carbon tape then these samples were gold sputtered for analysis by SEM. Images were taken at different magnification. Higher magnification was not possible because of breaking of the polymer at magnification greater than 10,000X.

Trapezium-X Universal Testing Machine (AG-20KNXD Plus) constructed by Shimadzu Corporation was used to determine tensile properties with a crosshead speed of 1mm/minute. Samples for these tests were prepared by cutting films in 10 mm x 50 mm (width x length) dimensions and a hand cutter (ASTM D6287) was used for 20 mm of gauge length.

Swelling analysis of the nanocomposites was carried out by taking 10mm x 10mm strips of nanocomposites films in a pre-weighed Eppendorf tube. To this, added 1ml of PBS and Eppendorf tube was placed in an incubator set at 37^{o}C for 1 month. At day 1, 2, 5, 7, 14, 20 and 24 media was changed and to measure increase in weight, strips were dried and then placed at weighing balance. Weight percent was calculated and resultant data was plotted against time. Swelling ratio of the samples were calculated by following formula:

$$S = [(W_s – W_d) / W_d] \times 100$$

Where W_d and W_s are the weights of the dried and swollen samples.

Biocompatibility of these blends were assessed by MTT assay, for which Vero cell lines were taken. These frozen cell lines were passed through a solution five times containing (Dulbecco's modified eagle medium) DMEM along with 10% (fetal bovine serum) FBS, and 1% Penstrep. These samples were then incubated at body temperature and followed by incubation, bypassed humidified air comprising 5% CO_2. Culture medium was altered every following day and cells were allowed to process through after confluence of 70%. All sample blends were cut into discs of 15mm diameter, followed by disinfection with 70% ethanol for 2h. Prior to carrying out in vitro analysis, those were further washed with (phosphate buffer solution) PBS and colonized on sterilized 24 well plate and compressed. Cell lines were seeded onto the samples with 1×10^4 cells/well strength. Vero cell lines

were cultivated in the aforementioned DMEM medium for 1, 3 and 7 days. 10% PrestoBlue which is a cell viability reagent was first grown in DMEM and then cultivated onto cells for 2h. After that, 100uL of cyto-viability reagent was transferred onto 96 well plate. Cell viability was calculated by placing the plate on plate reader for which 535-560nm is fluorescence intensity of excitation and 590-615 nm of emission. This assay was run in triplicates in three independent experiments.

Chapter 4

4 Results and Discussion:

4.1 Structure of the Nanocomposites:

4.1.1 Morphology of the Nanoparticles and Nanocomposites films:

nHA and nWH were observed under SEM to visualize their morphology and size. Morphology of nHA and nWH appeared spherical with aspect ratio zero, while size of HA was 23-40nm and WH existed in 17-23nm range.

Lab synthesized PCL, PCL/MCC, PC5 nanocomposites prepared by solvent casting method were observed under SEM to understand the morphology and dispersion of MCC and nanoparticles in PCL based films. Both surface and cryofractured surface images were captured under various magnifications to understand the surface and internal structure of MCC and nanoparticles embedded PCL films as shown in Figure 4.1. Pristine PCL films have a porous morphology and homogeneous features indicating the crystalline structure of PCL as shown in Figure 4.1 c) and d). Upon addition of the MCC in the PCL at different weight percentages, we observed homogeneous dispersion of MCC up to 5 wt % and there was no sign of phase separation. MCC rods were observed to have sharp and defined edges. It is vivid from Figure 4.1 e) MCC are embedded in the PCL matrix giving its surface rough topography. Moreover, addition of MCC into the polymer matrix lead to a reduction in the pore size/voids due to interfacial bonding between two polymers. As concentration of MCC was gradually increased in the composites from 5% to 15%, empty spaces were gradually

filled which is attributed lowering of surface energy which promotes higher cohesion of PCL and MCC [64].

On the introduction of inorganic fillers in the organic matrix, significant changes in the morphology of composites are detected as ceramic nanoparticles are exposed to empty pores surface of the matrix. In case of PC5-nHA, a homogeneous distribution of HA nanoparticles in PCL matrix while in case of the PC5-nWH, we observed that some area of the films have slight agglomerates of the WH nanoparticles in some partial locations. Although the incorporation of HA and WH nanoparticles in the polymer matrix significantly influenced the surface topography of the thin films, Nanocomposites were prepared successfully with homogeneous and uniform distribution of nanoparticles. Both nanoparticles further reduced the pore size of the composites by filling the empty spaces which was a consequence of enhanced coherence and extensive networking between filler and base material. Due to compact and dense structure, film thickness was reduced to 142.80 µm and 138.57 µm, when HA and WH were mounted as filler in 1-10% w/w concentrations respectively. As polymer chains entangled with each other pleats were

formed and surface became coarse. These entanglements act as stress transforming points [20]

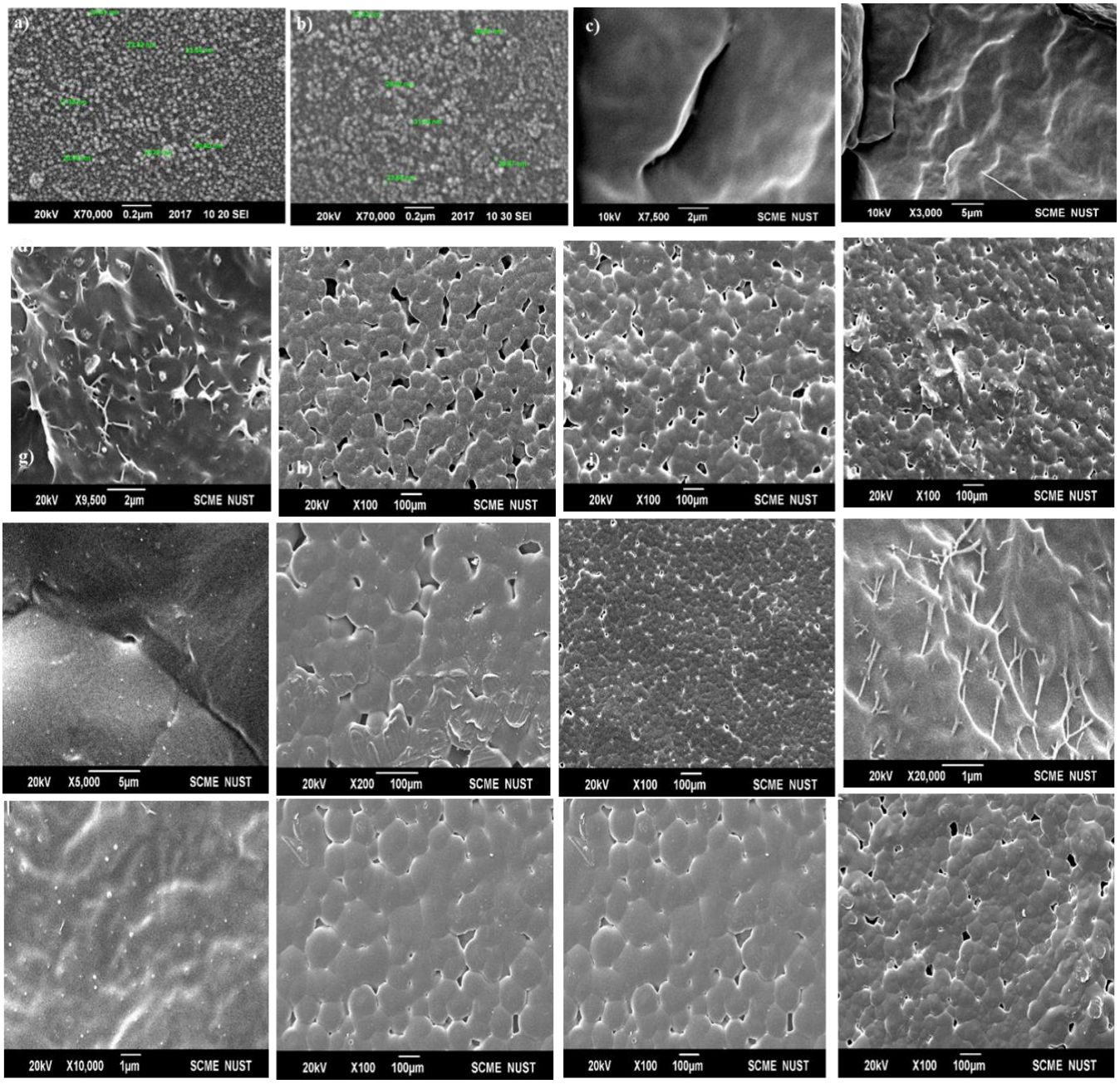

Figure 4.1 SEM images of a) nHA b) WH, c-d) PCL, e-h) PCL/Cellulose (5-15%), i-l) PCL/Cellulose/nHA (1-10%) , and m-p) PCL/Cellulose/nWH (1-10%) …...; 0.1

µm and X100,000; SEM images of. Nanocomposites. Scale bar = 1-100µm and the images were taken at 20 kV.

4.1.2 Wide angle XRD of the Nanoparticles and Nanocomposites films:

XRD was carried out for the phase confirmation of the synthesized nanoparticles. XRD pattern shown in Figure 3 a) has characteristic diffraction peaks of nHA at 2 Theta 25.8°, 31.9°, 32.9, 34.0° and 39.8° corresponding to crystal planes of HA (002), (211), (300), (202) and (310), respectively matches the JCPDS 09-0432 and is in accordance with the already reported data [65, 66]. Crystallite size of synthesized nanoparticles by using Scherer formula was found to be 22.3nm. For synthesized whitlockite nanoparticles diffraction peaks are witnessed at two theta of 44.16°, 37.72°, 34.56°, 32.9°, 31.32°, 28.02°, 25.96°and 17.1° representing crystallographic planes (220), (0210), (330), (214), (1010), and (100) of WH. Crystallite size was found to be 19 nm and homogenous phase distribution of WH is confirmed according to JCPDS 70-2064 [67, 68].

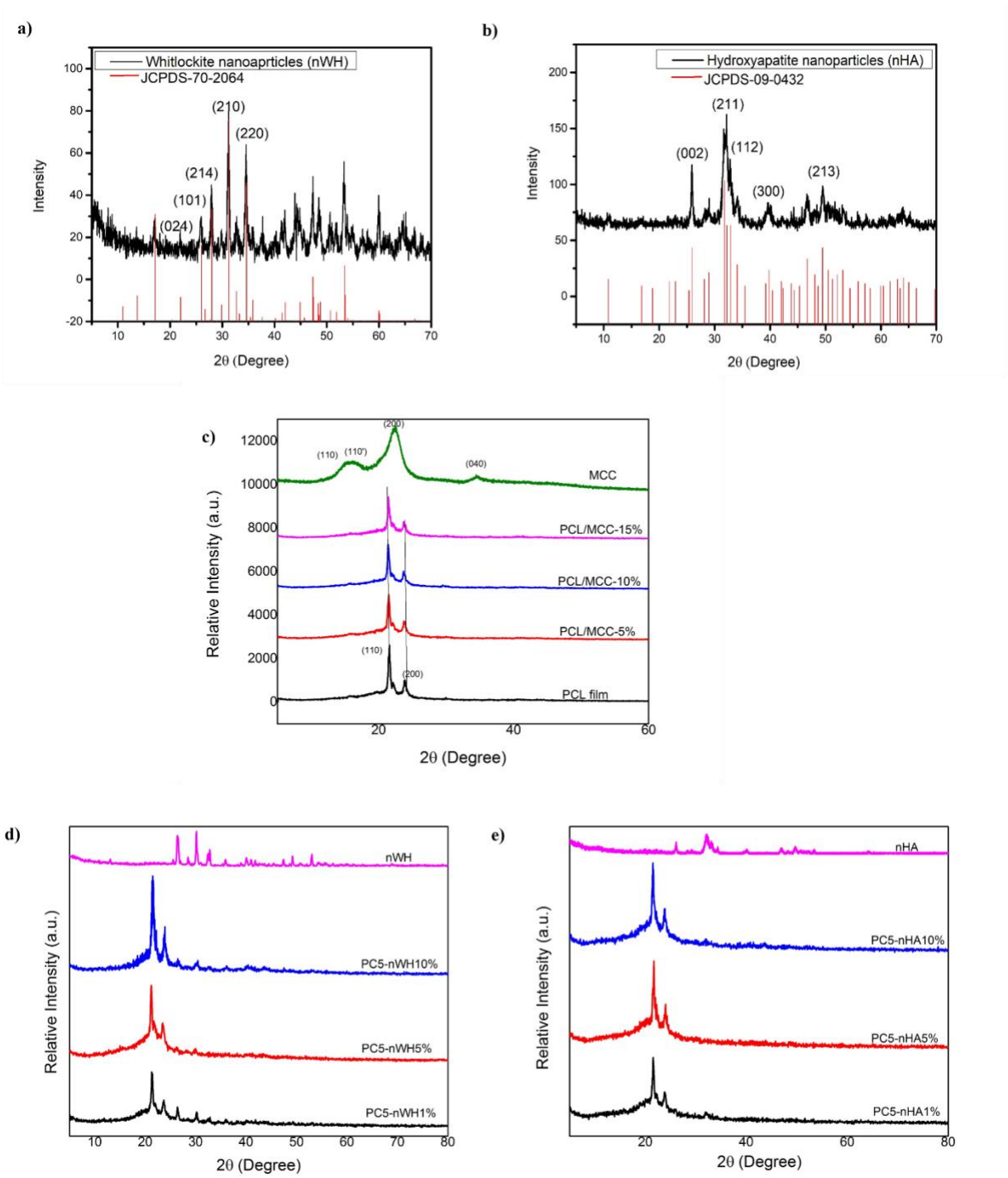

Figure 4.2 XRD spectra a) nWH b) nHA c) PCL/MCC blends d) PC5/nWH nanocomposites e) PC5/nHA nanocomposites

PCL exhibited two different peaks at 21.5^{o} and 24^{o} at 2θ indicating 110 and 200 crystallographic planes respectively and shoulder peak at 22^{o} [69]. MCC peaks were observed at 14^{o}, 16^{o}, 22.5^{o}, 34^{o} corroborating with the planes (110), (001), (200), and (004) respectively [70]. As MCC is loaded onto PCL, an increase in the peak shoulder of 22.5^{o} is observed whose peak intensified on increasing MCC loading and a significant change in the crystal structure of the blends is observed. Upto to 5% addition of MCC, an increase in the peak intensity is seen which can be attributed to the nucleation caused by MCC resulting in increase in crystallinity of the composites/blends. But with 10-15% content of MCC a gradual reduction in the peak intensity and area under the peak is observed which implies decrease in the crystallinity, cause MCC interrupts the crystal structure of the polymer [71].

After addition of nHA 1%, 5% and 10% in the PCL-MCC blend of 95%-5% w/w concentration respectively, it was observed that PCL peaks at 2θ = 22^{o} and 24^{o} remained intact and an additional peak at 2θ = 31.8^{o} appeared corresponding to 211 plane of the apatite particles. The sharpness and strength of nHA peak was increased with the increase in the concentration of nHA, suggesting gradual upsurge in the crystallinity of the nanocomposites. At 10% addition of nHA particles, a small peak at 26.05^{o} which tallies with the 002 reflective plane of nHA is also observed. For the nWH addition in the PCL-MCC blends, peaks for nWH are observed at 26.5^{o}, 28.6^{o}, 30.3^{o}, and 32.9^{o} which matches with the (214), (300), (0210) and nWH (220) crystal planes of, in addition to PCL peaks at 22^{o} and 24^{o}. As the amount of nWH and nHA nanoparticles is increased from 1-10% w/w, a gradual increase in the intensity of the peaks is observed, which implies that these particles act as nucleating agents causing improved alignment, closer packing and

orientation for the PCL-MCC films which further results in the improved crystallinity of the matrices.

4.1.3 FTIR analysis of the Nanoparticles and Nano composite films:

FTIR was carried out to check interaction between inorganic filler and organic polymer matrix in nanocomposites. No chemical degradation of the any constituent materials is indicated in FTIR spectra. FTIR is used to identify functional group present in the nanocomposites as well as to analyze the chemical change between nano composite after mixing. The synthesized nHA compound was subjected to FTIR. The presence of peaks at 1092 (PO_4^{3-}, ν_1), 1023 (PO_4^{3-}, ν_1), 963 (OH^{-1}), 601 (HPO_4^{2-}), and 561 cm^{-1} (PO_4^{3-}, ν_3) were the characteristic bands for nHA [72]. A very small peak of OH is visible at 3571cm^{-1}. It can be interested that the amount of H_2O is very low. Particularly, band at 963 cm^{-1} was distinguishable peak observed for asymmetric P-O stretching vibration of PO_4^{3-}. In addition, medium sharp peak appeared at 631 cm^{-1} corresponds to O-H deformation mode. FTIR bands for nWH is shown in Figure 2b). Characteristic vibrational bands of nWH were observed at 571 cm^{-1} and 582 cm^{-1} double peak (v4, bending of PO_4^{3-}), very 989 cm^{-1} (v1,P-O-H stretching of HPO_4^{2-}), 884cm^{-1}(v3, HPO_4^{2-} bending) , and 1059 cm^{-1} (v3 of PO_4^{3-}) bending [73-75]. Relatively sharp peak at 1346 is assigned to P(O-H) [76] while two bands at 2374 and 2794 cm^{-1} are assigned to P-O overtone on the basis of previous reports [74].

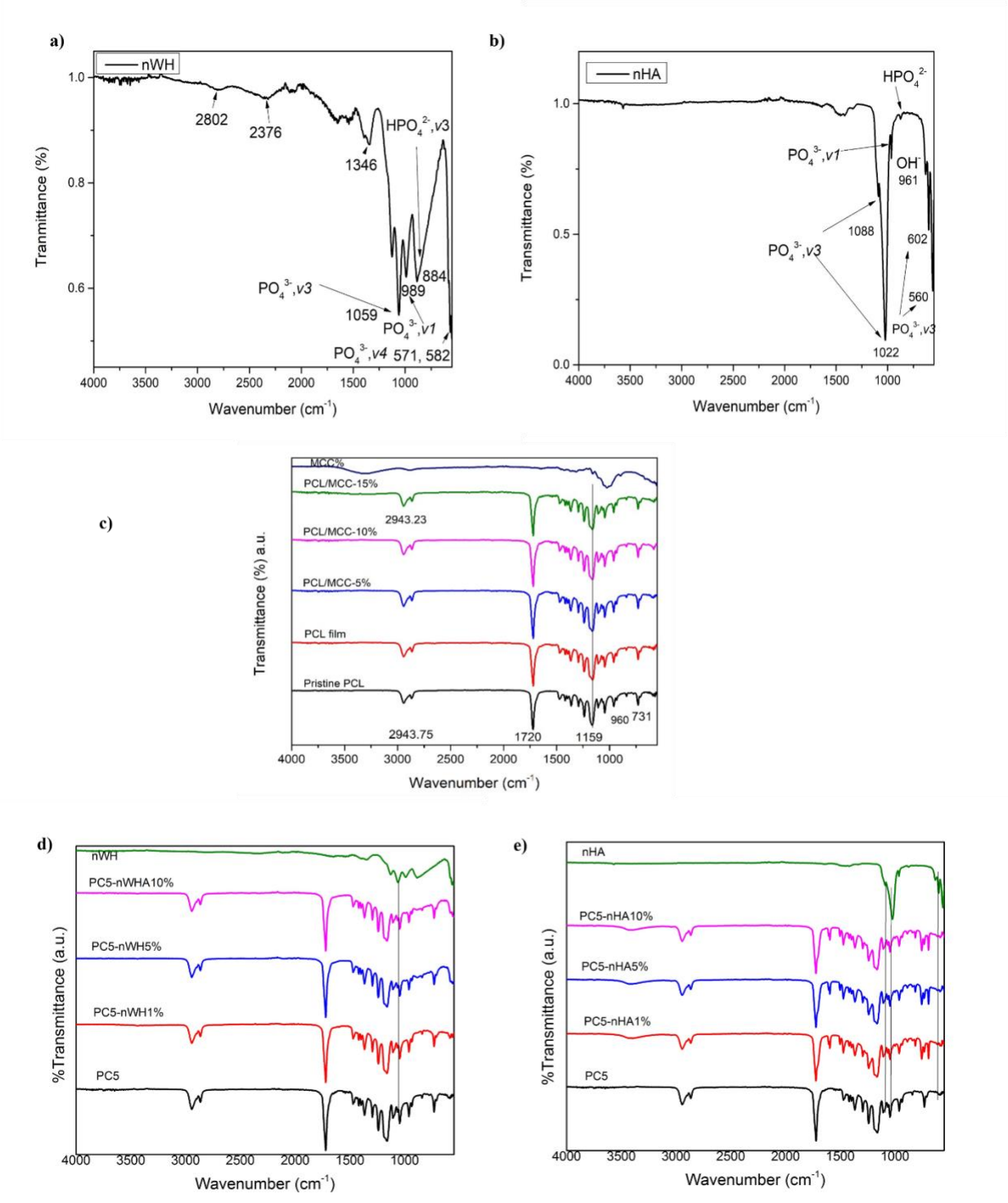

Figure 4.3 FTIR spectra a) nWH b) nHA c) PCL/MCC blends d) PC5/nWH nanocomposites e) PC5/nHA nanocomposites

FTIR of neat microcrystalline cellulose showed a broad peak at 3333 cm^{-1} and a small peak at 1636 cm^{-1} due to stretching of hydrogen bonded OH groups on the surface. A band at 2905 cm^{-1} corresponded to the asymmetric bending of C-H functional group. Owing to the C-O group vibration, a strong absorption band was observed at ca. 1050 cm^{-1} [77].

FTIR analysis of both pristine PCL and PCL film were performed and similar spectra were obtained. Peaks at 2943 cm^{-1}, 2865 cm^{-1}, 1720 cm^{-1}, 1240 cm^{-1} (crystalline phase of PCL), 1159 cm^{-1} (amorphous phase of PCL), attributed to the asymmetric v_{as} stretching of CH_2, symmetric CH_2 v_s stretching, C=O bending of ester group, COC asymmetric bending, and symmetric stretching of C-O-C respectively, were characteristic bands of PCL. A stronger intensity band corresponding to the amorphous phase, and consistent with the XRD analysis [78].

On addition of MCC to PCL, typical peak of cellulose disappeared due to dehydration and the expected reaction between carbonyl group of PCL and hydroxyl group of MCC did not occur which lead to non-displacement in the carbonyl peak. But the peak areas of CH_2 and C-O-C groups reduced on the cellulose loading, which suggested the augmentation in the crystallinity of PCL on the gradual loading of MCC [79].

Upon the addition of HA in 1%, 5%, and 10% wt/wt percentage, characteristic PCL bands are observed at 2943 cm^{-1}, 2865 cm^{-1} and 1720 cm^{-1}, along with characteristic PO_3^{-4} peaks at 561cm^{-1} while the peak at 1023 cm^{-1} is shifted towards greater wavenumber 1044 cm^{-1} and 1092 cm^{-1} is shited at 1110 cm^{-1}. New bands at 1591 cm^{-1}, 1503 cm^{-1} and 821 cm^{-1} appear confirming the chemical interaction between PCL and nHA. The overall intensity of the PCL bands is reduced upon the incorporation of nHA.

On the incorportion of nWH in PCL, characteristic PCL vibrational bands are intact with slight reduction in their intensity. Characteristic WH bands at 989 cm^{-1} and 884 cm^{-1} are not apparent when WH concentration is 1% but when its content is increased to 5-10% it becomes prominent and shifts towrds lower wavenumber, while one at 1067 cm^{-1} is merged in the PCL bands.

4.2 Thermo mechanical Properties of the Nanocomposites:

4.2.1 Thermal Analysis of Nanocomposites films:

4.2.1.1 Thermo gravimetric analysis *(*TGA*)* and Differential thermal analysis *(*DTA*):*

To check the thermal stability of the nanocomposites and change in weight percentage, TGA was conducted by heating at constant rate. TGA is also helpful in determining the maximum temperature that scaffolds can bear in thermal processing and their homogeneity. Thermograms from TGA/DTA of PCL/MCC blends and nanocomposites are shown in Figure 4.5. Pristine PCL shows thermal degradation in one step at 373 ^{o}C which is consistent with the previously reported in literature [80] with 89.1 % mass loss. However, incorporation of cellulose caused a significant increase in the degradation temperature of PCL. These composites showed two step thermal degradation depending upon the weight percentages of PCL and MCC. In case of nanocomposites, final residues were found at ---- proving that composites have completely degraded. Here, the weight loss was similar to the MCC and HA/WH concentrations. To the best of our knowledge, this is first study of PCL reinforced with MCC and further addition of different concentrations of HA and WH.

In addition, an upsurge in the thermal stability is observed for 5%, 10% and 15% incorporation of MCC with mass loss of 92.8%, 91.31%, and 93.7% respectively. Maximum thermal stability is observed when MCC concentration is 5% w/w, and 10%,

while for 15% a gradual decrease is observed but still better than PCL alone. The melting point of PCL increased on the incorporation of MCC. This increased thermal stability can be attributed to the positive interactions between MCC and PCL. Due the hydrogen bond formation b/w carbonyl groups of PCL and hydroxyl groups of MCC, dehydration of MCC is delayed and char and gasses formed by the degradation of cellulose react with the solid PCL causing improved thermal stability. So MCC acts as stabilizer which explains increment in the thermal stability [81]. With the increment of nHA and nWH in PCL-MCC5 matrix, onset temperature of thermal decomposition and maximum degradation temperature are enhanced thus establishing that nHA and nWH act as reinforcing agent.

The inclusion of nHA and nWH showed a significant variation in the stability of the product. In case of nHA composites, mass loss upto 200 ^{o}C is due to removal of absorbed water and lattice water while mass loss upto 456 ^{o}C is attributed to the decomposition of hydrogen phosphate ions to pyrophosphate ions. By comparing the relative thermal stabilities of the composites, it is concluded that incorporation of HA improves their thermal stability.

Table 4.1. Representing the *TGA* and *DTA* values of PCL/MCC blend and PC5/nHA and PC5/nWH Nanocomposites

.

Polymer System	Sample Code	TGA curve Temp. (^{o}C)		DTA curve Temp. (^{o}C)		Loading of nHA(g) /nWH
PCL	PC	373	-	417	447	-
PCL/MCC-5%	PC5	395	461	399	465	-
PCL/MCC-10%	PC10	390	447	406	451	-
PCL/MCC-15%	PC15	383	439	390	435	-
PCL/MCC-5%-nHA1%	PC5-HA1	-	-	-	-	0.01
PCL/MCC-5%-nHA5	PC5-HA5	393	451	399	456	0.05
PCL/MCC-5%-nHA10%	PC5-HA10	395	449	386	458	0.10
PCL/MCC-5%-nWH1%	PC5-WH1	-	-	-	-	0.01
PCL/MCC-5%-nWH5%	PC5-WH5	392	458	401	456	0.05
PCL/MCC-5%-nWH10%	PC5-WH10	385	447	400	425	0.10

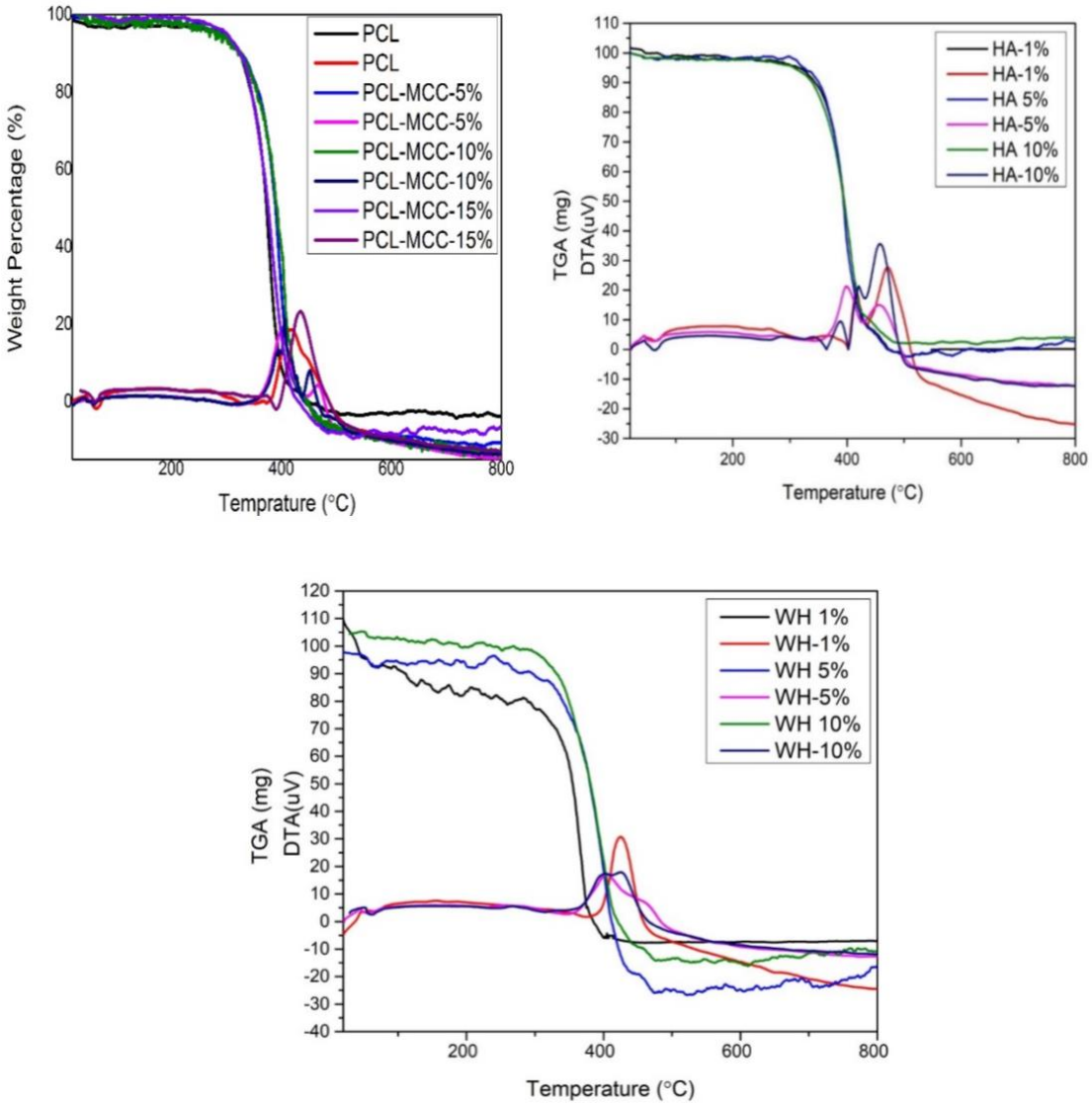

Figure 4.4 Thermal Analysis of PCL/Cellulose, PCL/Cellulose/nWH, and PCL/Cellulose/nHA

4.2.1.2 Differential Scanning calorimetry:

DSC of the polymeric nanocomposites is conducted to better understand their crystallinity and structure. DSC thermograms for the first heating scan, cooling scan and second heating

scan are presented in Figure 4.6 and thermal parameter obtained from these curves are summarized in table 4.2.

In general, melting temperature values (T_{m1} °C, T_{m2} °C) and cooling crystallization temperature (T_{cc} °C) values of PCL-MCC blends suffered minor decreases and shifted to lower values as compared to the of pristine PCL. In the first heating curve, T_{m1} values decrease from 64.1 °C for pure PCL to 63.59 °C for 5 wt% MCC, 63.39 °C for 10 wt% MCC, 62.54 °C for 15 wt% MCC and T_{m2} values from second heating curve decreased from 56 °C for neat PCL to 55.58 °C for 5 wt% MCC, 55.58 °C for 10 wt% MCC, 55.50 °C for 10 wt% MCC and 55.48 °C for 15 wt% MCC. T_{cc} values obtained from cooling crystallization curve first lowered from 30.74 °C for pristine PCL to 28.91 °C for 5 wt% MCC, then increased to 29.41 °C for 10 wt% MCC and 30.17 °C for 15 wt% MCC. This decrease in the values of T_{cc} , T_{m1} , T_{m2} on the addition of MCC can be explained on the fact that it interrupts the crystal structure and molecular and chain mobility of the polymer .

The degree of crystallinity showed opposite trend as on the inclusion of MCC, a gradual increase in the crystallinity was observed while, maximum crystallinity was witnessed with PC5. The X_c value increased form 17% for pure PCL to 19% for 5 wt% MCC, 18.5% for 10 wt% MCC and 18% for 15 wt% MCC. The calorimetric findings are consistent with XRD and FTIR analysis of polymer blends and can be attributed to the reinforcement and nucleation effect of the filler particles. When concentration of the MCC particles reaches

upto 10-15%, due to lack of interaction with matrix and availability of low interfacial area hinders it to act as nucleating agent and consequently prevents increment in crystallinity.

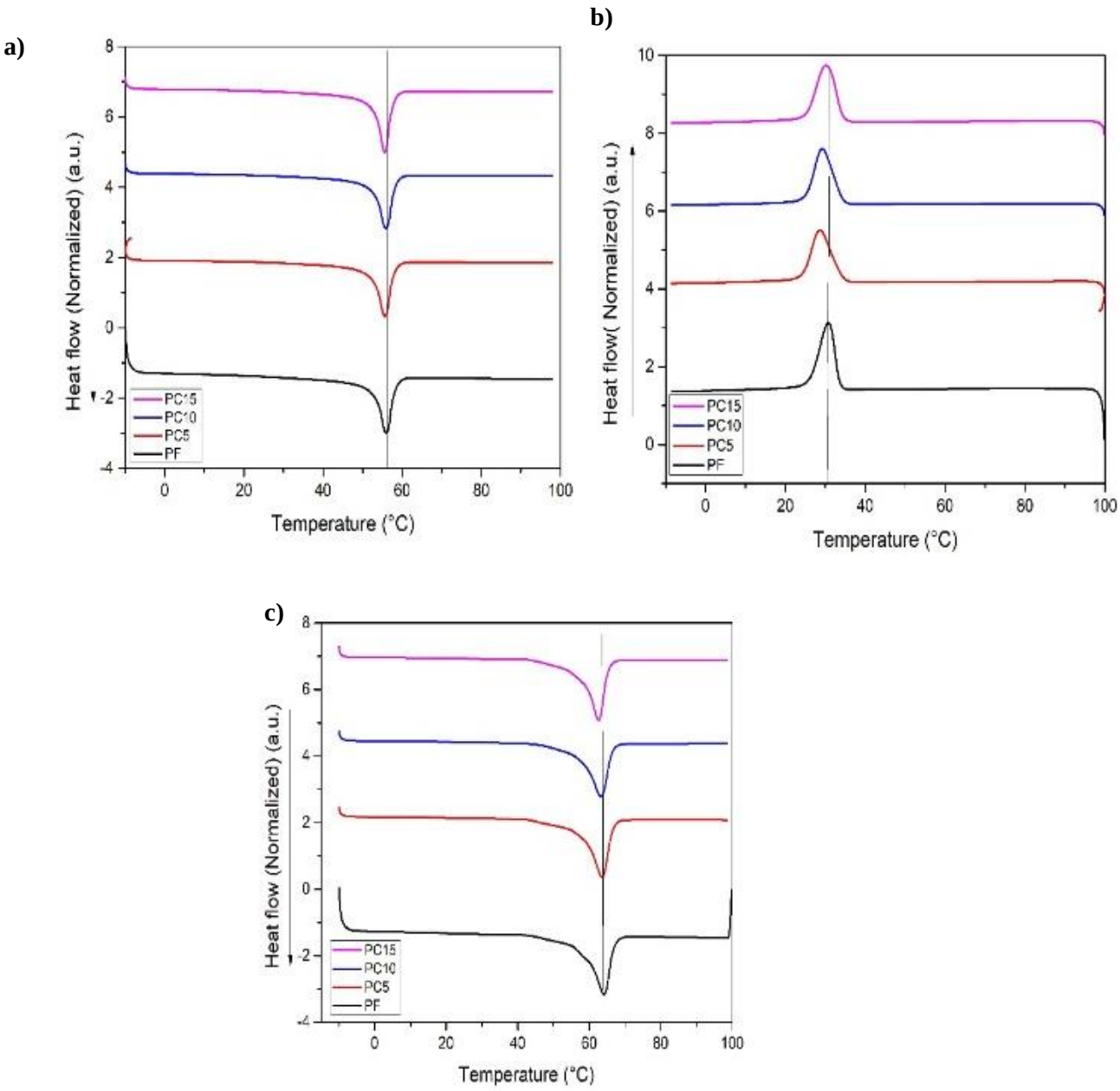

Figure 4.5. DSC analysis of PCL, PCL-MCC blends at the heating rate of 10°C/min a) first heating curve b) cold crystallization curve c) second heating curve

Table 4.2. Representing the T_m, T_c, and degree of crystallinity X_c (%) values of PCL/MCC blend.

Sample Code	T_{m1} (°C)	T_{cc} (°C)	T_{m2} (°C)	X_c (%)
PF	64.1	30.74	56	17
PC5	63.59	28.91	55.58	19
PC10	63.39	29.41	55.50	18.5
PC15	62.54	30.17	55.48	18

4.2.2 Mechanical properties:

Figure 6 shows stress-strain curves obtained from tensile mechanical testing of PCL, PCL/MCC with different loadings of MCC (5%, 10%, and 15%) wt/wt concentration. Different parameters obtained from stress-strain curves are detailed in Table 3. PCL is a rigid polymer having high tensile strength but breaks at the elongation value of 355% strain. From these curves, it can be interpreted that when 5% concentration of MCC was added to the PCL, a substantial increase in the ultimate tensile strength, elongation at break point and Young's Modulus was observed, which is in contrast to when 10% and 15% of MCC was added. Tensile mechanical properties are dependent on the matrix and filler weight percent. The tensile modulus of PCL/MCC 5% is increased by ~ 106% from 888.27±1.21 to 938±1.45MPa, elongation at break point also increased by ~ 152% from 355.29 to 541.63. When 10% MCC is added ultimate tensile strength values decreased by ~ 67% from 6.56 to 4.45 MPa and Modulus was reduced by ~ 92% from 888.27±1.21 to 824±2.0 while, the elongation at break point increased by 122% than pure PCL. Similarly, when 15% MCC was added in the pure PCL system Young's Modulus lowered by ~ 96% from 888.27±1.21 MPa to 852±0.05 MPa, strain % reduced by ~ 49% from 355.29 to 173.9 and UTS values drastically reduced by ~153% from 6.56 to 4.27 MPa. This implies that addition of MCC in PCL is showing saturation in effect and thus, tensile Modulus and

ultimate tensile strength are decreasing but still we have better elongation at break as compare to PCL. Upon reaching 15% MCC concentration, mechanical properties decreased drastically. This decrease in the mechanical properties can be attributed to the decrease in the nucleation effect and increase in crystallinity. When filler concentration exceeds limit value (10%), particles start to agglomerate owing to the lack of interaction with the matrix which lead to decrease in the interfacial area acting as point of nucleation thus, causing brittleness [82]. These agglomerates not only weaken the composite material but also impedes layer to layer adhesion.

When HA and WH were incorporated into composite films in 1%, 5%, and 10% w/w percentage, a substantial increase in all mechanical characteristics was witnessed. Figure 7 shows the stress-strain curve of tensile testing of HA1, HA5, HA10, WH1, WH5, and WH10 respectively and compared with the pristine PCL and PCL-MCC5. Values of different mechanical parameters are enlisted in table 3. For 1%, 5%, 10% addition of HA, modulus increased from 938MPa to 954.25MPa, 996MPa, and 1004.26MPa respectively and elongation at break augmented from 435.87% to 537%, 571%, 695%, while the UTS values decreased 6.35MPa from to 4.9MPa, 5.1MPa, and 5.8MPa. When WH was inserted in same fraction as of HA, strain percent value enhanced from 435% to 501%, 629% and 833% and UTS amplified from 6.35MPa to 7.2MPa, 8.1MPa, and 8.2MPa, while tensile Modulus values enlarged from 938MPa to 923.25MPa, 980.45MPa and 1115.91MPa. This lowering in the UTS values is due to agglomeration of n-HA and n-WH particles in the polymer matrix which is owing to absence of hydrogen bonding between filler and polymer matrix. It is observed that nanoparticles distribution is homogenous and random in nanocomposites. While, an incessant increase in the tensile strength is attributed to the

synergistic effect of filler and matrix as filler inhabits pores of matrix and load is shifted to the filler and it acts as reinforcing agent [83]. The bonding of the nanoparticles with the polymer matrix can lead to retardation, interruption and even blockage of the micro crack formation and propagation. The intimate interaction between polymer matrix and nanoparticles results in enlargement of matrix's local stress which is then transferred to the nanoparticles. Hence, inclusion of nanoparticles can delay or interrupt the expansion and growth of cracks by stress distribution. Furthermore, these inorganic fillers also enhanced density and crystallization of the polymer which is useful for improving hardness of the composites [84]. Cancellous bone requires the elastic modulus of 0.1-4.5GPa, while that of cortical bone is 17 GPa [85] . Depending upon these values of mechanical testing above mentioned films are a good candidate for the cancellous bone tissue engineering and dressing application. Specifically, these nanocomposites can be used as in mechanically active area. Results revealed that mechanical properties of the polymers can be fine-tuned by changing the nanoparticle concentration in the nanocomposites.

a)

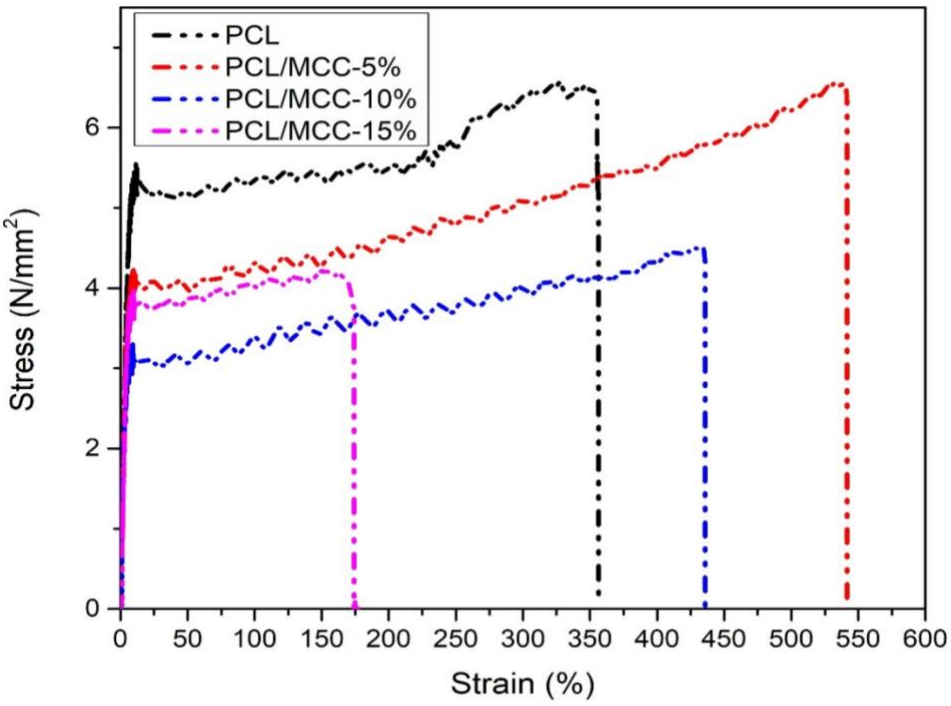
PCL
PCL/MCC-5%
PCL/MCC-10%
PCL/MCC-15%
Stress (N/mm^2)
Strain (%)
0
2
4
6
0 50 100 150 200 250 300 350 400 450 500 550 600

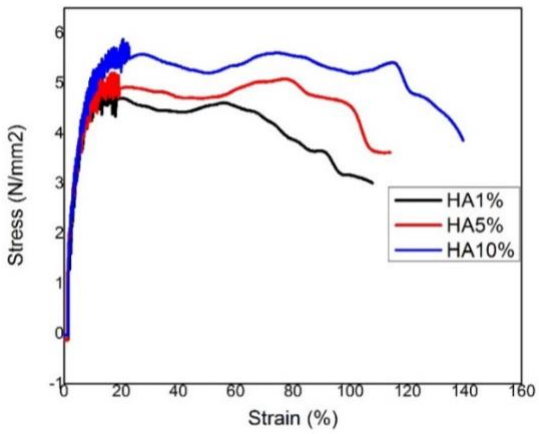
HA1%
HA5%
HA10%
Stress (N/mm2)
Strain (%)
0 20 40 60 80 100 120 140 160

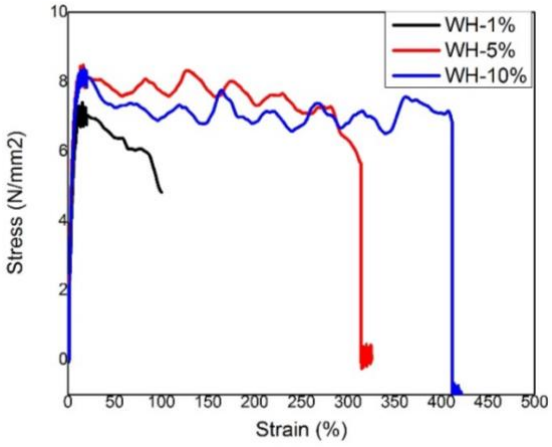
WH-1%
WH-5%
WH-10%
Stress (N/mm2)
Strain (%)
0 50 100 150 200 250 300 350 400 450 500

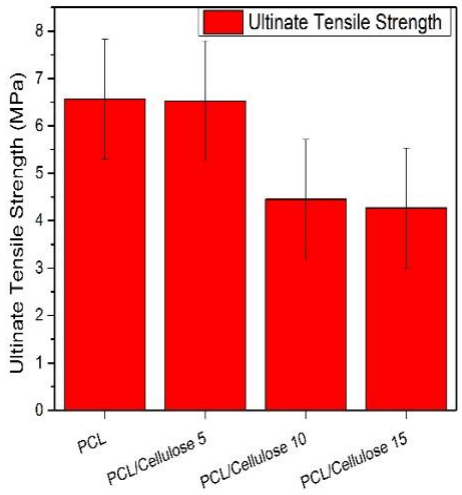
Ultinate Tensile Strength
Ultinate Tensile Strength (MPa)
0
1
2
3
4
5
6
7
8
PCL
PCL/Cellulose 5
PCL/Cellulose 10
PCL/Cellulose 15

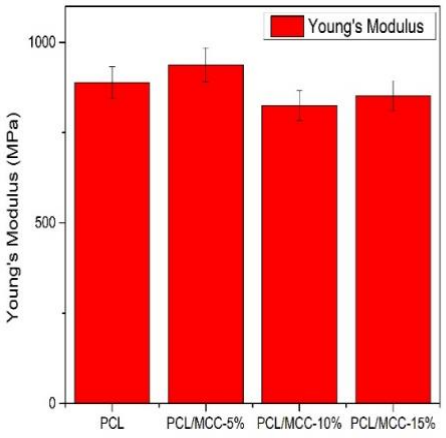
Young's Modulus
Young's Modulus (MPa)
0
500
1000
PCL
PCL/MCC-5%
PCL/MCC-10%
PCL/MCC-15%

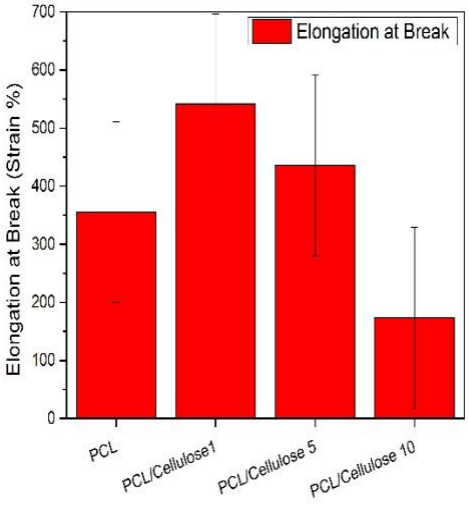
Elongation at Break
Elongation at Break (Strain %)
0
100
200
300
400
500
600
700
PCL
PCL/Cellulose1
PCL/Cellulose 5
PCL/Cellulose 10

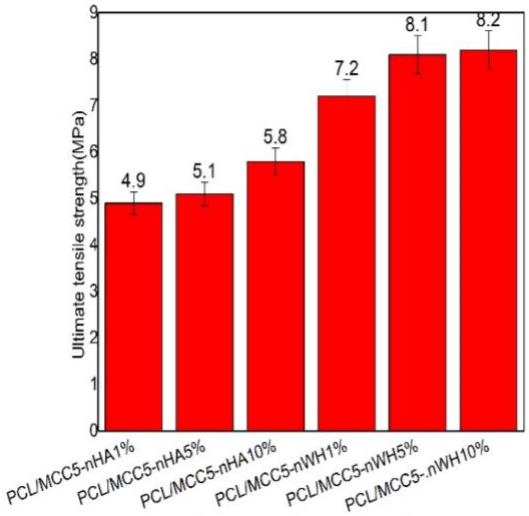
Ultimate tensile strength(MPa)
0
1
2
3
4
5
6
7
8
9
4.9
5.1
5.8
7.2
8.1
8.2
PCL/MCC5-nHA1%
PCL/MCC5-nHA5%
PCL/MCC5-nHA10%
PCL/MCC5-nWH1%
PCL/MCC5-nWH5%
PCL/MCC5-nWH10%

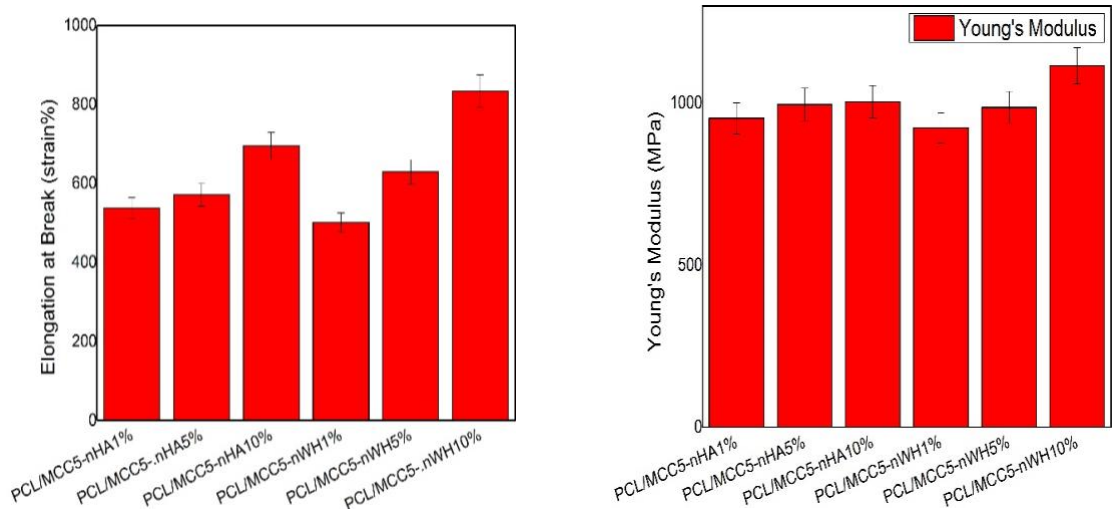

Figure 4.6 Mechanical properties Stress strain curves of PCL/Cellulose, PCL/Cellulose/nWH, and PCL/Cellulose/nHA Ultimate tensile strength of PCL/Cellulose, PCL/Cellulose/nWH, and PCL/Cellulose/nHA, Young's modulus of PCL/Cellulose, PCL/Cellulose/nWH, and PCL/Cellulose/nHA Elongation at break PCL/Cellulose, PCL/Cellulose/nWH, and PCL/Cellulose/nHA

. Data is statistically significant (Error bars: ±SD, * p b 0.05, **p b 0.01, and ***p b 0.001)

Table 4.3: Showing the a) young modulus, b) strain (%), and c) maximum Stress of PCL/MCC Blends

a)

Composite Formulation	**Young Modulus (MPa)**	**Elongation at Break Strain %**	**UTS Maximum Stress (MPa)**

PCL	888±1.21	355.29	6.56
PCL/Cellulose 5	938±1.45	541.63	6.53
PCL/Cellulose 10	824±2.0	435.87	4.45
PCL/Cellulose 15	852±0.05	173.9	4.27

Table 4.4 Showing the a) young modulus, b) strain (%), and c) maximum Stress of PCL/MCC/nHA and PCL/MCC/nWH nanocomposites.

	Young Modulus with nHA nd nWH (MPa)	**Elongation at Break with nHA and nWH**	**UTS with nHA and nWH**
PCL/Cellulose5-nHA1%	954.25	537	4.9
PCL/Cellulose5-nHA5%	996.87	571	5.1
PCL/Cellulose5-.nHA10%	1004.26	695	5.8
PCL/Cellulose5-nWH1%	923.25	501	7.2
PCL/Cellulose5-nWH5%	980.45	629	8.1
PCL/Cellulose5-.nWH10%	1115.91	833	8.2

4.3 Nanocomposites as a Biomimetic scaffold:

4.3.1 Swelling Analysis:

Swelling properties of the pristine PCL, PCL-MCC blends and nanocomposites of PCL-MCC with nHA and nWH were studied until equilibrium was achieved. Swelling analysis helps to understand surface, mass transfer properties and solvent diffusion as it depends on the network density and polymer structure. During the assessment of scaffolds for their application in tissue engineering, swelling behavior is an important index because inadequate solvent absorption hinders cell growth and excessive absorption leads to destruction of scaffold's morphology [86]. The neat PCL shows high dimensional stability than PCL-MCC blends due to its semi crystalline and hydrophobic nature which implies that in the semi distorted arrangement of PCL chains no sufficient spaces are present to accommodate solvent molecules. While, with the addition of MCC an increasing trend in the swelling behavior is observed which can be attributed to the OH groups present on the MCC surface [87].

Addition of nHA and nWH upto 10% in the blends lead to further escalation in swelling ratio and improved nanocomposites' fidelity. This indicated that nanoparticles anchor polymeric chains firmly in their neighborhood, eventually leading towards enhanced network density. This cross-linked networking and hydrophilic moieties not only enhances integrity of the nanocomposites, but also is a prime factor in growth of swelling ratio [88]. A dramatic change is observed in first 24 hours and after that equilibrium is achieved.

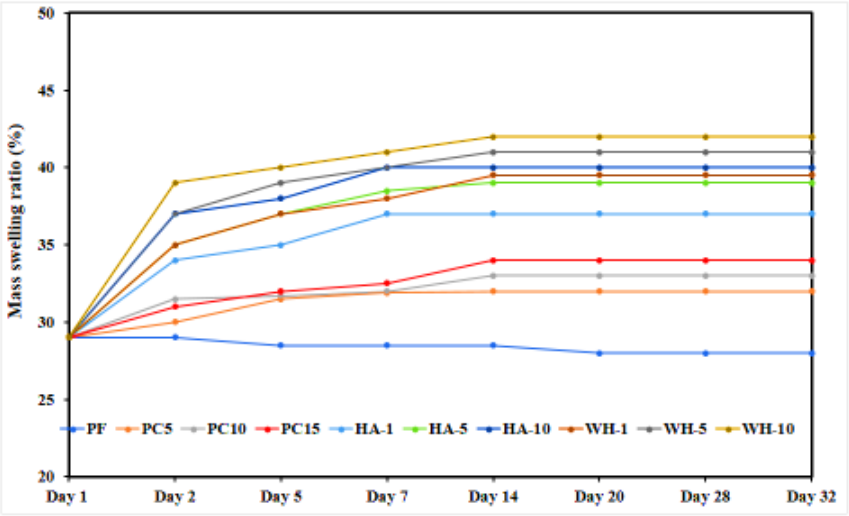

Figure 4.8- Mass swelling behavior of the nanocomposites with respect to time.

4.3.2 Cell culture:

We designed PCL/MCC blends decorated with nWH and nHA for bone regeneration scaffold. For the introduction of any material as a scaffold in the tissue engineering it's important to study their cytocompatibility profile. Vero cell lines were cultured on the surface of PCL, PCL-MCC blends and PCL/MCC nanocomposites with nHA and nWH to understand the cell adhesion and viability studies as shown in Figure 4.9. From the cell viability it is clear that the pristine nanoparticles have cell viability ~70.66 % and ~72.30 % for nHA and nWH while pristine PCL has ~86.56%. These nanoparticles were composited with PC5, the cell viability of the resulting nanocomposites is higher than the pristine nanoparticles. In case of PCL/MCC blends the highest cell viability is shown by PC5 which is around 87.75%. On further addition of MCC in PCL at 10 and 15 wt% cell

viability decreased from pristine PCL. Addition of nWH and nHA in PC5, increased the cell viability on the scaffold surface. In case of the PC5/nWH, addition of the nanoparticles cell viability amplified as compared to pristine PCL and PC5. In case of HA all the nanocomposites showed cell viability more than 90%. From these cytocompatibility results it may be assessed that there was no compromise on biocompatibility according to standard ISO 10993-5:2009. Introduction of the nanoparticles and MCC in PCL caused an increase in the hydrophilicity of scaffold resulting in increased cellular viability on the scaffold surface.

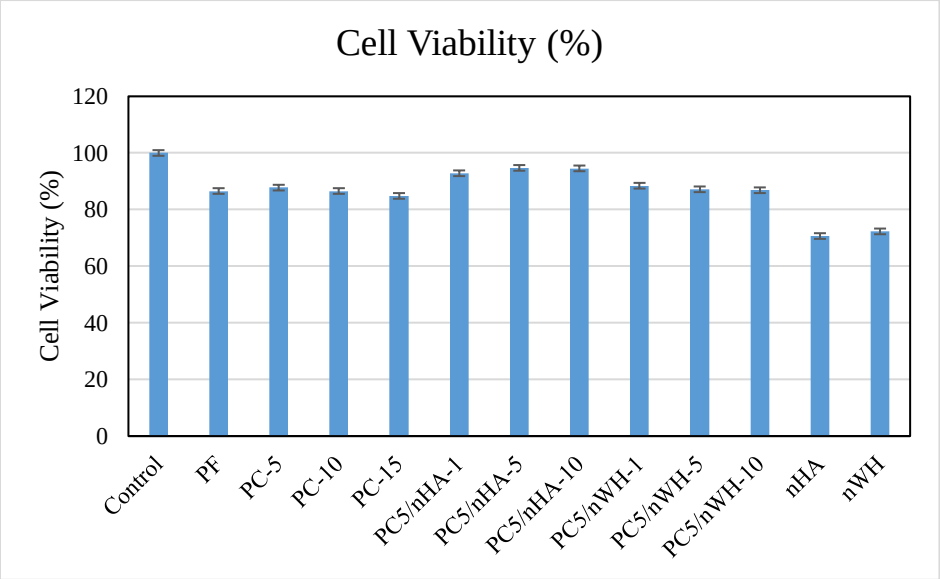

Figure 4.7- Cell viability calculation of nanocomposites. Data is statistically significant.

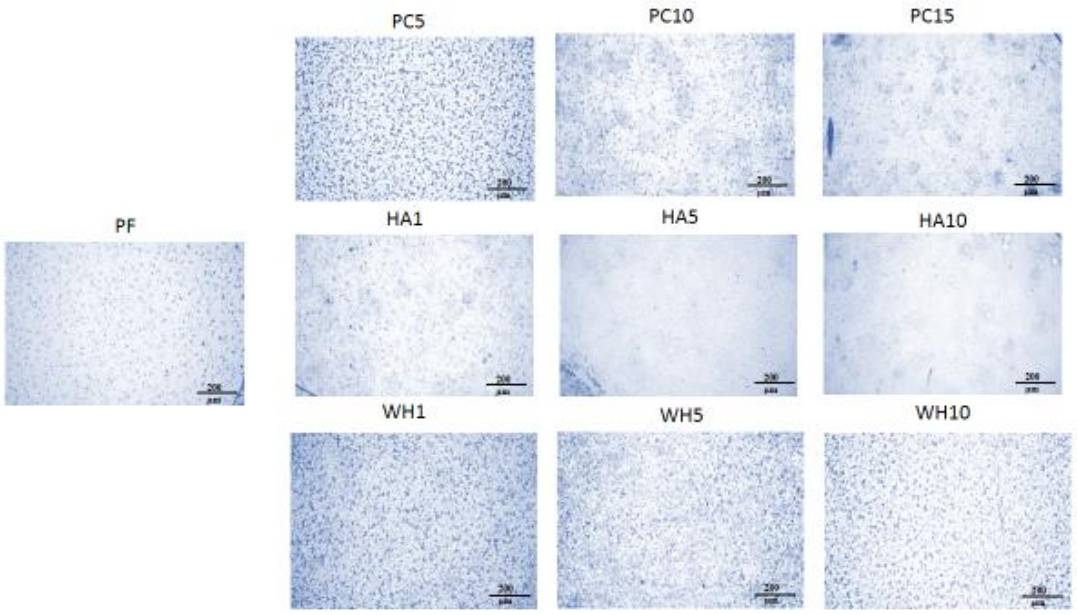

Figure 4.8- Cell adhesion images of the nanocomposites stained with crystal violet.

Cellular morphology and adhesion in the surface of the films was studied by taking the phase contrast images after staining the cells with crystal violet as shown in Figure 4.10. Cells showed branched and interconnected network with morphology suggesting successful cell adhesion and proliferation on the surface of the scaffold. In case of the nanocomposites the cells population on the surface of the scaffold increased demonstrating that nanoparticles provided cell anchoring sites which magnified cellular function. From the PC5/nWH it is clear that cells are well anchored on the scaffold surface and these results corroborate the cell viability results.

Live dead assay was performed on nano-composites by using NIH3T3-L1 cell lines and dual acridine orange/ethidium bromide (AO/EB) fluorescent staining, visualized under a fluorescent microscope, is used to identify apoptosis-associated changes of cell membranes during the process of apoptosis. Live cells are detected as green fluorescence

by acridine orange indicating intracellular esterate activity, and dead cells are detected as red fluorescence when ethidium homodimer binds to DNA. Ethidium homodimer is excluded from live cells because of cell membrane integrity, while in dead cells, loss of plasma membrane activity allows ethidium homodimer entering cells and binding to DNA. Live/Dead Assay revealed the live/dead cells proportion in the culture medium.

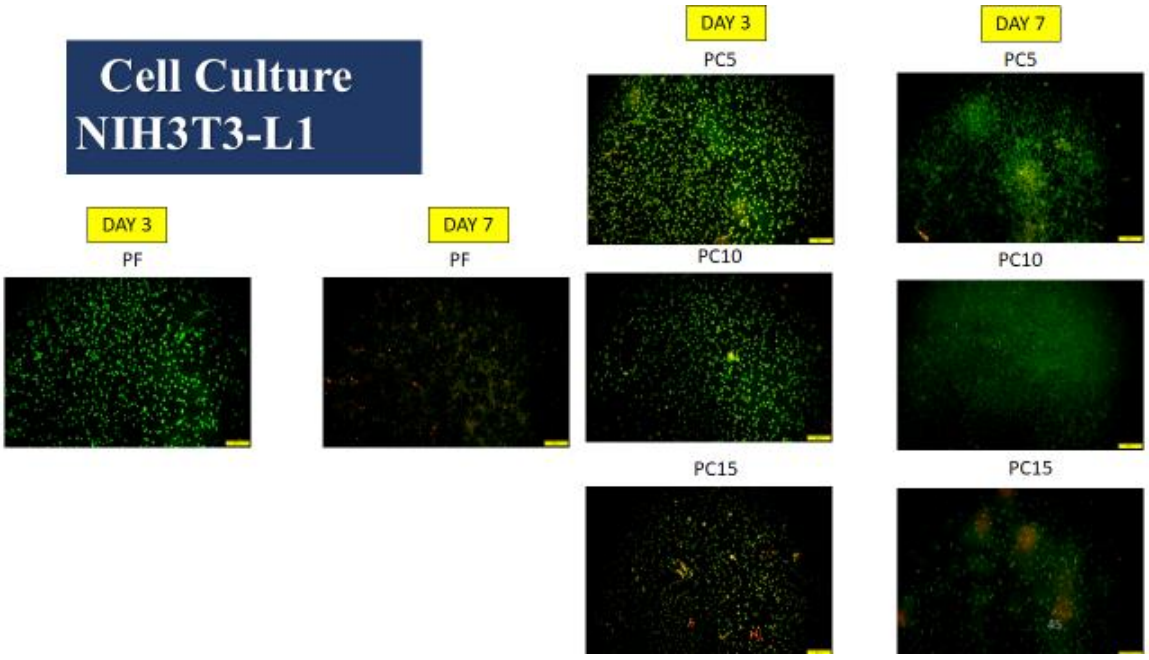

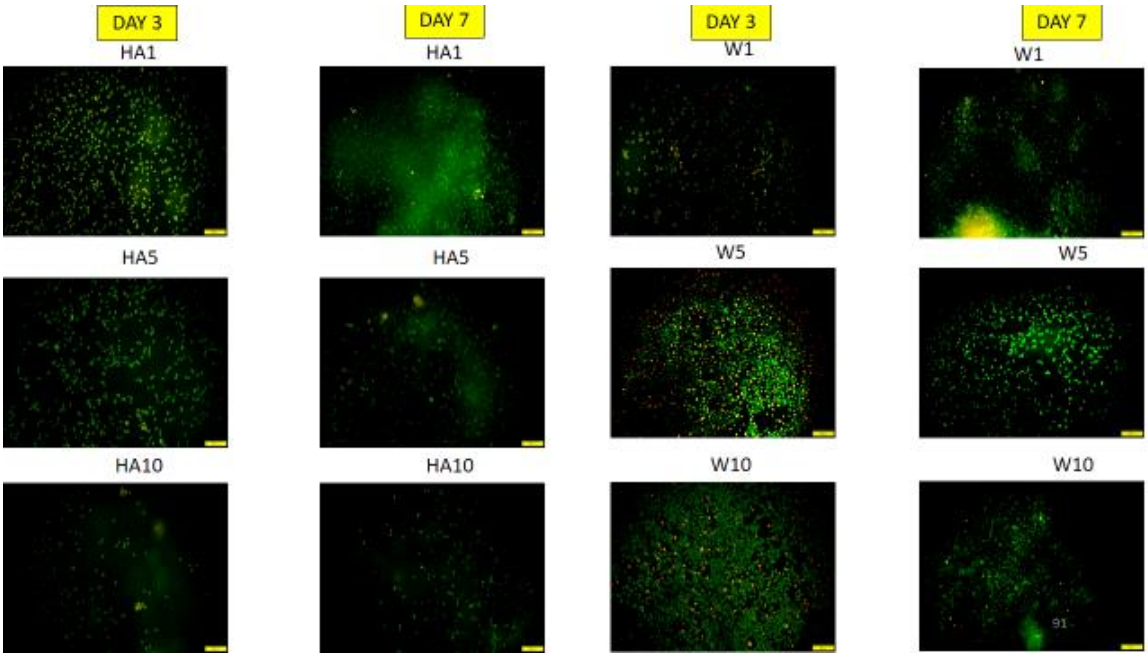

Figure 4.9- Live Dead Assay of NIH3t3-L1 cell lines for day 3 and day 7

Conclusion:

Novel biomimetic nanocomposites of PCL/MCC-5 embedded with different weight loadings of nHA and nWH were prepared for bone repair and regeneration applications. SEM images showed that nanoparticles are homogeneously dispersed in the base matrix upto 5 wt% and above that agglomeration occurred. Upon the addition of nanoparticles, mechanical properties of the composites were drastically increased. nWH containing nanocomposites showed enhanced tensile strength as compared to that of nHA and such improvement in the strength and stiffness of the hybrid nanocomposites is the pre requisite of sample fidelity. The bioactivity of the composites was studied on vero cell line for 3 days. The nanocomposites containing composites showed improved cell adhesion as compare to the PCL/MCC-5 blends which implies that functional moieties of the nHA/nWH breed anchoring situates for the cell adhesion which is required for forming the interconnected cellular network of bone.

1. References:

1. Hassan, M.E.S., J. Bai, and D.-Q. Dou, *Biopolymers; definition, classification and applications.* Egyptian Journal of Chemistry, 2019. **62**(9): p. 1725-1737.
2. Pradhan, R.A., et al., *Biopolymers.* 2021: p. 281-303.
3. Cerri, B.C., et al., *Evaluation of new environmental friendly particulate soil fertilizers based on agroindustry wastes biopolymers and sugarcane vinasse.* Waste Management, 2020. **108**: p. 144-153.
4. Qureshi, D., et al., *Introduction of biopolymers: food and biomedical applications*, in *Biopolymer-Based Formulations*. 2020, Elsevier. p. 1-45.
5. Andreeßen, C. and A. Steinbüchel, *Recent developments in non-biodegradable biopolymers: Precursors, production processes, and future perspectives.* Applied microbiology and biotechnology, 2019. **103**(1): p. 143-157.
6. Feng, P., et al., *Characterizations and interfacial reinforcement mechanisms of multicomponent biopolymer based scaffold.* Materials Science and Engineering: C, 2019. **100**: p. 809-825.
7. Kimura, K. and Y. Oki, *Efficient control of membrane fouling in MF by removal of biopolymers: Comparison of various pretreatments.* Water research, 2017. **115**: p. 172-179.
8. Gutiérrez, T.J. and K. Álvarez, *Biopolymers as microencapsulation materials in the food industry.* Advances in physicochemical properties of biopolymers: Part, 2017. **2**: p. 296-322.
9. Wicochea-Rodríguez, J.D., et al., *Active food packaging based on biopolymers and aroma compounds: how to design and control the release.* Frontiers in chemistry, 2019. **7**: p. 398.
10. Jacob, J., et al., *Biopolymer based nanomaterials in drug delivery systems: A review.* Materials Today Chemistry, 2018. **9**: p. 43-55.
11. Reddy, M., et al., *A comparative review of natural and synthetic biopolymer composite scaffolds.* Polymers, 2021. **13**(7): p. 1105.
12. Bruggeman, K.F., R.J. Williams, and D.R. Nisbet, *Dynamic and responsive growth factor delivery from electrospun and hydrogel tissue engineering materials.* Advanced healthcare materials, 2018. **7**(1): p. 1700836.
13. Jordan, J., et al., *Experimental trends in polymer nanocomposites—a review.* Materials science and engineering: A, 2005. **393**(1-2): p. 1-11.
14. Drury, J.L. and D.J. Mooney, *Hydrogels for tissue engineering: scaffold design variables and applications.* Biomaterials, 2003. **24**(24): p. 4337-4351.
15. Boskey, A.L., *Bone composition: relationship to bone fragility and antiosteoporotic drug effects.* BoneKEy reports, 2013. **2**.
16. Jang, H.L., et al., *In Vitro and In Vivo Evaluation of Whitlockite Biocompatibility: Comparative Study with Hydroxyapatite and β-Tricalcium Phosphate.* Advanced healthcare materials, 2016. **5**(1): p. 128-136.
17. Kim, H.D., et al., *Biomimetic whitlockite inorganic nanoparticles-mediated in situ remodeling and rapid bone regeneration.* Biomaterials, 2017. **112**: p. 31-43.
18. Wozney, J.M., *Bone morphogenetic proteins.* Progress in growth factor research, 1989. **1**(4): p. 267-280.

19. Cheng, H., et al., *Synergistic interplay between the two major bone minerals, hydroxyapatite and whitlockite nanoparticles, for osteogenic differentiation of mesenchymal stem cells.* Acta biomaterialia, 2018. **69**: p. 342-351.
20. Hae Lin Jang†, K.J., Jaehun Lee†, Younghye Kim†, Seung Hoon Nahm‡, Kug Sun Hong†, and Ki Tae Nam†*, <*Revisiting whitlockite, the second most abundant biomineral in bone - nanocrystal synthesis in physiologically relevant conditions and biocompatibility evaluation (1).pdf*>. ACS publication, 2014.
21. Zhou, H. and J. Lee, *Nanoscale hydroxyapatite particles for bone tissue engineering.* Acta biomaterialia, 2011. **7**(7): p. 2769-2781.
22. Webster, T.J., R.W. Siegel, and R. Bizios, *Osteoblast adhesion on nanophase ceramics.* Biomaterials, 1999. **20**(13): p. 1221-1227.
23. Labet, M. and W. Thielemans, *Synthesis of polycaprolactone: a review.* Chemical society reviews, 2009. **38**(12): p. 3484-3504.
24. Park, S.A., S.H. Lee, and W.D. Kim, *Fabrication of porous polycaprolactone/hydroxyapatite (PCL/HA) blend scaffolds using a 3D plotting system for bone tissue engineering.* Bioprocess and biosystems engineering, 2011. **34**(4): p. 505-513.
25. Saji, V.S., H.C. Choe, and K.W. Yeung, *Nanotechnology in biomedical applications: a review.* International Journal of Nano and Biomaterials, 2010. **3**(2): p. 119-139.
26. Ramos, A.P., et al., *Biomedical applications of nanotechnology.* Biophysical reviews, 2017. **9**(2): p. 79-89.
27. Jordan, J., et al., *Experimental trends in polymer nanocomposites—a review.* Materials science and engineering: A, 2005. **393**(1-2): p. 1-11.
28. Drury, J.L. and D.J. Mooney, *Hydrogels for tissue engineering: scaffold design variables and applications.* Biomaterials, 2003. **24**(24): p. 4337-4351.
29. Hassan, M.E.S., J. Bai, and D.-Q. Dou, *Biopolymers; Definition, Classification and Applications.* Egyptian Journal of Chemistry, 2019. **62**(9): p. 1725-1737.
30. Pradhan, R.A., et al., *Biopolymers.* 2021: p. 281-303.
31. Cerri, B.C., et al., *Evaluation of new environmental friendly particulate soil fertilizers based on agroindustry wastes biopolymers and sugarcane vinasse.* Waste Management, 2020. **108**: p. 144-153.
32. Qureshi, D., et al., *Introduction of biopolymers: food and biomedical applications*, in *Biopolymer-Based Formulations*. 2020, Elsevier. p. 1-45.
33. Andreeßen, C. and A. Steinbüchel, *Recent developments in non-biodegradable biopolymers: Precursors, production processes, and future perspectives.* Applied microbiology and biotechnology, 2019. **103**(1): p. 143-157.
34. Feng, P., et al., *Characterizations and interfacial reinforcement mechanisms of multicomponent biopolymer based scaffold.* Materials Science and Engineering: C, 2019. **100**: p. 809-825.
35. Kimura, K. and Y. Oki, *Efficient control of membrane fouling in MF by removal of biopolymers: Comparison of various pretreatments.* Water research, 2017. **115**: p. 172-179.
36. Gutiérrez, T.J. and K. Álvarez, *Biopolymers as microencapsulation materials in the food industry.* Advances in physicochemical properties of biopolymers: Part, 2017. **2**: p. 296-322.

37. Wicochea-Rodríguez, J.D., et al., *Active food packaging based on biopolymers and aroma compounds: how to design and control the release.* Frontiers in chemistry, 2019. **7**: p. 398.
38. Jacob, J., et al., *Biopolymer based nanomaterials in drug delivery systems: A review.* Materials Today Chemistry, 2018. **9**: p. 43-55.
39. Reddy, M., et al., *A comparative review of natural and synthetic biopolymer composite scaffolds.* Polymers, 2021. **13**(7): p. 1105.
40. Bruggeman, K.F., R.J. Williams, and D.R. Nisbet, *Dynamic and responsive growth factor delivery from electrospun and hydrogel tissue engineering materials.* Advanced healthcare materials, 2018. **7**(1): p. 1700836.
41. Labet, M. and W. Thielemans, *Synthesis of polycaprolactone: a review.* Chemical society reviews, 2009. **38**(12): p. 3484-3504.
42. Park, S.A., S.H. Lee, and W.D. Kim, *Fabrication of porous polycaprolactone/hydroxyapatite (PCL/HA) blend scaffolds using a 3D plotting system for bone tissue engineering.* Bioprocess and biosystems engineering, 2011. **34**(4): p. 505-513.
43. Zhang, C., et al., *Incorporation of poly (ethylene glycol) grafted cellulose nanocrystals in poly (lactic acid) electrospun nanocomposite fibers as potential scaffolds for bone tissue engineering.* Materials Science and Engineering: C, 2015. **49**: p. 463-471.
44. Chen, G., et al., *A novel thermoformable bionanocomposite based on cellulose nanocrystal-graft-poly (ε-caprolactone).* Macromolecular Materials and Engineering, 2009. **294**(1): p. 59-67.
45. Boskey, A.L., *Bone composition: relationship to bone fragility and antiosteoporotic drug effects.* BoneKEy reports, 2013. **2**.
46. Jang, H.L., et al., *In Vitro and In Vivo Evaluation of Whitlockite Biocompatibility: Comparative Study with Hydroxyapatite and β-Tricalcium Phosphate.* Advanced healthcare materials, 2016. **5**(1): p. 128-136.
47. Kim, H.D., et al., *Biomimetic whitlockite inorganic nanoparticles-mediated in situ remodeling and rapid bone regeneration.* Biomaterials, 2017. **112**: p. 31-43.
48. Wozney, J.M., *Bone morphogenetic proteins.* Progress in growth factor research, 1989. **1**(4): p. 267-280.
49. Cheng, H., et al., *Synergistic interplay between the two major bone minerals, hydroxyapatite and whitlockite nanoparticles, for osteogenic differentiation of mesenchymal stem cells.* Acta biomaterialia, 2018. **69**: p. 342-351.
50. Hae Lin Jang†, K.J., Jaehun Lee†, Younghye Kim†, Seung Hoon Nahm‡, Kug Sun Hong†, and Ki Tae Nam†*, <*Revisiting whitlockite, the second most abundant biomineral in bone - nanocrystal synthesis in physiologically relevant conditions and biocompatibility evaluation (1).pdf*>. ACS publication, 2014.
51. Zhou, H. and J. Lee, *Nanoscale hydroxyapatite particles for bone tissue engineering.* Acta biomaterialia, 2011. **7**(7): p. 2769-2781.
52. Webster, T.J., R.W. Siegel, and R. Bizios, *Osteoblast adhesion on nanophase ceramics.* Biomaterials, 1999. **20**(13): p. 1221-1227.
53. Cheng, H., et al., *Synergistic interplay between the two major bone minerals, hydroxyapatite and whitlockite nanoparticles, for osteogenic differentiation of mesenchymal stem cells.* Acta Biomater, 2018. **69**: p. 342-351.

54. Jang, H.L., et al., *In Vitro and In Vivo Evaluation of Whitlockite Biocompatibility: Comparative Study with Hydroxyapatite and beta-Tricalcium Phosphate.* Adv Healthc Mater, 2016. **5**(1): p. 128-36.
55. Yu, X., et al., *Preparation of Poly(ether-ether-ketone)/Nanohydroxyapatite Composites with Improved Mechanical Performance and Biointerfacial Affinity.* ACS Omega, 2020. **5**(45): p. 29398-29406.
56. Cakmak, A.M., et al., *3D Printed Polycaprolactone/Gelatin/Bacterial Cellulose/Hydroxyapatite Composite Scaffold for Bone Tissue Engineering.* Polymers (Basel), 2020. **12**(9).
57. Nyberg, E., et al., *Comparison of 3D-Printed Poly-varepsilon-Caprolactone Scaffolds Functionalized with Tricalcium Phosphate, Hydroxyapatite, Bio-Oss, or Decellularized Bone Matrix<sup/>*. Tissue Eng Part A, 2017. **23**(11-12): p. 503-514.
58. Jing, X., H.Y. Mi, and L.S. Turng, *Comparison between PCL/hydroxyapatite (HA) and PCL/halloysite nanotube (HNT) composite scaffolds prepared by co-extrusion and gas foaming.* Mater Sci Eng C Mater Biol Appl, 2017. **72**: p. 53-61.
59. Yan, D., et al., *Study on the properties of PLA/PBAT composite modified by nanohydroxyapatite.* Journal of Materials Research and Technology, 2020. **9**(5): p. 11895-11904.
60. Chen, B. and K. Sun, *Mechanical and dynamic viscoelastic properties of hydroxyapatite reinforced poly(ε-caprolactone).* Polymer Testing, 2005. **24**(8): p. 978-982.
61. Salerno, A., et al., *Processing/structure/property relationship of multi-scaled PCL and PCL-HA composite scaffolds prepared via gas foaming and NaCl reverse templating.* Biotechnology and Bioengineering, 2011. **108**(4): p. 963-976.
62. Park, S.A., S.H. Lee, and W.D. Kim, *Fabrication of porous polycaprolactone/hydroxyapatite (PCL/HA) blend scaffolds using a 3D plotting system for bone tissue engineering.* Bioprocess Biosyst Eng, 2011. **34**(4): p. 505-13.
63. Chuenjitkuntaworn, B., et al., *Polycaprolactone/hydroxyapatite composite scaffolds: preparation, characterization, and in vitro and in vivo biological responses of human primary bone cells.* J Biomed Mater Res A, 2010. **94**(1): p. 241-51.
64. Biscaia, S.I., et al., *Production and Characterisation of PCL/ES Scaffolds for Bone Tissue Engineering.* Materials Today: Proceedings, 2015. **2**(1): p. 208-216.
65. Catledge, S.A., et al., *An electrospun triphasic nanofibrous scaffold for bone tissue engineering.* Biomed Mater, 2007. **2**(2): p. 142-50.
66. Gomez-Lizarraga, K.K., et al., *Polycaprolactone- and polycaprolactone/ceramic-based 3D-bioplotted porous scaffolds for bone regeneration: A comparative study.* Mater Sci Eng C Mater Biol Appl, 2017. **79**: p. 326-335.
67. Totaro, A., et al., *PCL-HA microscaffolds for in vitro modular bone tissue engineering.* J Tissue Eng Regen Med, 2017. **11**(6): p. 1865-1875.
68. Wutticharoenmongkol, P., et al., *Novel bone scaffolds of electrospun polycaprolactone fibers filled with nanoparticles.* J Nanosci Nanotechnol, 2006. **6**(2): p. 514-22.
69. Sousa, I., A. Mendes, and P.J. Bártolo, *PCL Scaffolds with Collagen Bioactivator for Applications in Tissue Engineering.* Procedia Engineering, 2013. **59**: p. 279-284.
70. Aleman-Dominguez, M.E., et al., *Three-dimensional printed polycaprolactone-microcrystalline cellulose scaffolds.* J Biomed Mater Res B Appl Biomater, 2019. **107**(3): p. 521-528.

71. Qian, Y., et al., *Fabrication and Characterization of Electrospun Polycaprolactone Blended with Chitosan-Gelatin Complex Nanofibrous Mats.* Journal of Nanomaterials, 2014. **2014**: p. 1-7.
72. Dietmar W. Hutmacher, 2 Thorsten Schantz,1 Iwan Zein,3 Kee Woei Ng,1 Swee Hin Teoh,1 Kim Cheng Tan4, *Mechanical properties and cell cultural response of polycaprolactone scaffolds designed and fabricated via fused deposition modeling.* © 2001 John Wiley & Sons, Inc, 2000.
73. Shirzaei Sani, I., et al., *Preparation and characterization of polycaprolactone/chitosan-g-polycaprolactone/hydroxyapatite electrospun nanocomposite scaffolds for bone tissue engineering.* Int J Biol Macromol, 2021. **182**: p. 1638-1649.
74. Mi, H.-Y., et al., *Poly(ε-caprolactone) (PCL)/cellulose nano-crystal (CNC) nanocomposites and foams.* Cellulose, 2014. **21**(4): p. 2727-2741.
75. Shkarina, S., et al., *3D biodegradable scaffolds of polycaprolactone with silicate-containing hydroxyapatite microparticles for bone tissue engineering: high-resolution tomography and in vitro study.* Sci Rep, 2018. **8**(1): p. 8907.
76. Basile, M.A., et al., *Functionalized PCL/HA nanocomposites as microporous membranes for bone regeneration.* Materials Science and Engineering: C, 2015. **48**: p. 457-468.
77. Kim, H.D., et al., *Biomimetic whitlockite inorganic nanoparticles-mediated in situ remodeling and rapid bone regeneration.* Biomaterials, 2017. **112**: p. 31-43.
78. Bauer, L., et al., *Bone-mimetic porous hydroxyapatite/whitlockite scaffolds: preparation, characterization and interactions with human mesenchymal stem cells.* Journal of Materials Science, 2020. **56**(5): p. 3947-3969.
79. Huang, S.H., et al., *Fabrication and characterization of polycaprolactone and tricalcium phosphate composites for tissue engineering applications.* J Dent Sci, 2017. **12**(1): p. 33-43.
80. Yang, Y., et al., *Microstructure evolution and texture tailoring of reduced graphene oxide reinforced Zn scaffold.* Bioact Mater, 2021. **6**(5): p. 1230-1241.
81. Arrieta, M.P., et al., *Electrospinning of PCL-Based Blends: Processing Optimization for Their Scalable Production.* Materials (Basel), 2020. **13**(17).
82. Spiridon, I., et al., *Development and Performance of Bioactive Compounds-Loaded Cellulose/Collagen/Polyurethane Materials.* Polymers (Basel), 2020. **12**(5).
83. Rasheed, M., et al., *Morphology, Structural, Thermal, and Tensile Properties of Bamboo Microcrystalline Cellulose/Poly(Lactic Acid)/Poly(Butylene Succinate) Composites.* Polymers (Basel), 2021. **13**(3).
84. Heydari, Z., D. Mohebbi-Kalhori, and M.S. Afarani, *Engineered electrospun polycaprolactone (PCL)/octacalcium phosphate (OCP) scaffold for bone tissue engineering.* Materials Science and Engineering: C, 2017. **81**: p. 127-132.
85. Amin, S., et al., *Synthesis and Characterization of Nano Hydroxyapatite using Reverse Micro Emulsions as Nano Reactors.* Journal of the Chemical Society of Pakistan, 2015. **37**(1).
86. Jang, H.L., et al., *Revisiting whitlockite, the second most abundant biomineral in bone: nanocrystal synthesis in physiologically relevant conditions and biocompatibility evaluation.* ACS nano, 2014. **8**(1): p. 634-641.

87. Jang, H.L., et al., *Phase transformation from hydroxyapatite to the secondary bone mineral, whitlockite.* Journal of Materials Chemistry B, 2015. **3**(7): p. 1342-1349.
88. Morouço, P., et al., *Fabrication of Poly (-caprolactone) Scaffolds Reinforced with Cellulose Nanofibers, with and without the Addition of Hydroxyapatite Nanoparticles.* BioMed research international, 2016. **2016**.
89. Klinkaewnarong, J. and S. Utara, *Ultrasonic-assisted conversion of limestone into needle-like hydroxyapatite nanoparticles.* Ultrasonics sonochemistry, 2018. **46**: p. 18-25.
90. Nazir, F. and M. Iqbal, *Comparative Study of Crystallization, Mechanical Properties, and In Vitro Cytotoxicity of Nanocomposites at Low Filler Loadings of Hydroxyapatite for Bone-Tissue Engineering Based on Poly (l-lactic acid)/Cyclo Olefin Copolymer.* Polymers, 2021. **13**(22): p. 3865.
91. Chandran R, R., et al. *Evaluation of whitlockite through conventional hydrothermal method and its in-vitro erythrocyte compatibility and antibacterial activity*. in *AIP Conference Proceedings*. 2020. AIP Publishing LLC.
92. Nazir, F., L. Abbas, and M. Iqbal, *A comparative insight into the mechanical properties, antibacterial potential, and cytotoxicity profile of nano-hydroxyapatite and nano-whitlockite-incorporated poly-L-lactic acid for bone tissue engineering.* Applied Nanoscience, 2021.
93. Arrieta, M.P., et al., *Electrospinning of PCL-based blends: Processing optimization for their scalable production.* Materials, 2020. **13**(17): p. 3853.
94. Nazir, F. and M. Iqbal, *Synthesis, characterization and cytotoxicity studies of aminated microcrystalline cellulose derivatives against melanoma and breast cancer cell lines.* Polymers, 2020. **12**(11): p. 2634.
95. Alemán-Domínguez, M.E., et al., *Microcrystalline cellulose as filler in polycaprolactone matrices*, in *Industry 4.0–Shaping The Future of The Digital World*. 2020, CRC press. p. 240-245.
96. Gieroba, B., et al., *Collagen maturity and mineralization in mesenchymal stem cells cultured on the hydroxyapatite-based bone scaffold analyzed by ATR-FTIR spectroscopic imaging.* Materials Science and Engineering: C, 2021. **119**: p. 111634.
97. Kaliannagounder, V.K., et al., *Remotely controlled self-powering electrical stimulators for osteogenic differentiation using bone inspired bioactive piezoelectric whitlockite nanoparticles.* Nano Energy, 2021. **85**: p. 105901.
98. Capitelli, F., et al., *Neutron and XRD Single-Crystal Diffraction Study and Vibrational Properties of Whitlockite, the Natural Counterpart of Synthetic Tricalcium Phosphate.* Crystals, 2021. **11**(3): p. 225.
99. Wang, C., et al., *Synthesis and formation mechanism of bone mineral, whitlockite nanocrystals in tri-solvent system.* Journal of colloid and interface science, 2020. **569**: p. 1-11.
100. Cooper, M.A., et al., *Wopmayite, ideally Ca6Na3□ Mn (PO4) 3 (PO3OH) 4, a new phosphate mineral from the Tanco Mine, Bernic Lake, Manitoba: description and crystal structure.* The Canadian Mineralogist, 2013. **51**(1): p. 93-106.
101. Kunusa, W.R., et al. *FTIR, XRD and SEM analysis of microcrystalline cellulose (MCC) fibers from corncorbs in alkaline treatment*. in *Journal of Physics: Conference Series*. 2018. IOP Publishing.

102. Gómez-Lizárraga, K., et al., *Polycaprolactone-and polycaprolactone/ceramic-based 3D-bioplotted porous scaffolds for bone regeneration: A comparative study.* Materials Science and Engineering: C, 2017. **79**: p. 326-335.
103. Alemán-Domínguez, M.E., et al., *Three-dimensional printed polycaprolactone-microcrystalline cellulose scaffolds.* Journal of Biomedical Materials Research Part B: Applied Biomaterials, 2019. **107**(3): p. 521-528.
104. Simao, J.A., C.F. Bellani, and M.C. Branciforti, *Thermal properties and crystallinity of PCL/PBSA/cellulose nanocrystals grafted with PCL chains.* Journal of Applied Polymer Science, 2017. **134**(8).
105. Ruseckaite, R.A. and A. Jiménez, *Thermal degradation of mixtures of polycaprolactone with cellulose derivatives.* Polymer Degradation and Stability, 2003. **81**(2): p. 353-358.
106. Yang, S., et al., *The design of scaffolds for use in tissue engineering. Part I. Traditional factors.* Tissue engineering, 2001. **7**(6): p. 679-689.
107. Eftekhari, S., et al., *Fabrication and characterization of novel biomimetic PLLA/cellulose/hydroxyapatite nanocomposite for bone repair applications.* Materials Science and Engineering: C, 2014. **39**: p. 120-125.
108. Yu, X., et al., *Preparation of Poly (ether-ether-ketone)/Nanohydroxyapatite Composites with Improved Mechanical Performance and Biointerfacial Affinity.* ACS omega, 2020. **5**(45): p. 29398-29406.
109. Hickey, D.J., et al., *Adding MgO nanoparticles to hydroxyapatite–PLLA nanocomposites for improved bone tissue engineering applications.* Acta biomaterialia, 2015. **14**: p. 175-184.
110. Guo, Z., et al., *Characterization of biodegradable poly (lactic acid) porous scaffolds prepared using selective enzymatic degradation for tissue engineering.* RSC advances, 2017. **7**(54): p. 34063-34070.
111. Gaharwar, A.K., et al., *Highly extensible, tough, and elastomeric nanocomposite hydrogels from poly (ethylene glycol) and hydroxyapatite nanoparticles.* Biomacromolecules, 2011. **12**(5): p. 1641-1650.
112. Koupaei, N., A. Karkhaneh, and M. Daliri Joupari, *Preparation and characterization of (PCL-crosslinked-PEG)/hydroxyapatite as bone tissue engineering scaffolds.* Journal of Biomedical Materials Research Part A, 2015. **103**(12): p. 3919-3926.